

Performance of Linear Induction Motors  
Within an Automated Transit Network

A Project

Presented to

The Faculty of the Department of Mechanical Engineering

San José State University

In Partial Fulfillment

of the Requirements for the Degree

Master of Science

In

Mechanical Engineering

By

Erik Aylen

December 2014

©2014

Erik Aylen

ALL RIGHTS RESERVED

San José State University

The Undersigned Project Committee Approves the Project Titled

Performance of Linear Induction Motors

Within an Automated Transit Network

by

Erik Aylen

Approved for the Department of Mechanical Engineering

---

Dr. Burford Furman

Date

Committee Chair

---

Dr. Winncy Du

Date

Committee Member

---

Dr. Ping Hsu

Date

Committee Member

## **ABSTRACT**

This project examines the use of linear induction motors (LIMs) as the primary propulsion source for the Superway automated transit network (ATN). Current LIM applications are considered, and the feasibility and tradeoffs associated with the use of LIMs vs. more traditional rotary motors are explored. Aspects particular to automated transit vehicles are discussed. The effects on motor thrust of larger-than-specified air gap and LIM misalignment are described. An analytical model is presented and its output is compared with acceleration data from lab experiments. Some discussion of electrical efficiencies is included. This information is used to specify H2W Technology's LMG-06-650-SSE as a candidate to supply motive power for the Superway ATN.

The conclusion is drawn that a short-primary LIM is likely not practical for the Superway ATN, while a long-primary configuration should be able to meet system requirements.

## **ACKNOWLEDGEMENTS**

I would like to recognize Dr. Furman's consistent corrective efforts keeping me on track for this project. I have also received invaluable advice from my two other committee members, Dr. Du and Dr. Hsu, steering the course of my attention and keeping the scope ambitious but still achievable. And of course this project would have been a very different experience without the input and support of my financial sponsor, Ed Porter.

Without the understanding and seemingly inexhaustible support of my wonderful partner Shelley, I would have achieved nothing. I owe her a debt far greater than could fit on any page. All my thanks, and all my love.

# TABLE OF CONTENTS

ABSTRACT	iv
ACKNOWLEDGEMENTS	iv
TABLE OF CONTENTS	v
NOMENCLATURE	vii
LIST OF FIGURES	viii
1.0 INTRODUCTION	1
1.1 LITERATURE REVIEW	2
1.1.1 BACKGROUND	2
1.1.2 DC MACHINES	3
1.1.3 SYNCHRONOUS AC MACHINES	3
1.1.4 INDUCTION MACHINES	3
1.1.5 LINEAR INDUCTION MACHINES	4
1.1.5.1 ADVANTAGES OVER ROTARY MACHINES	5
1.1.5.2 DISADVANTAGES	7
1.1.5.3 AIR GAP CONSIDERATIONS	7
1.2 OPERATIONAL PRT SYSTEMS WORLDWIDE	9
1.2.1 TRANSIT SYSTEMS USING LIM PROPULSION	9
1.2.2 PRT SYSTEMS WORLDWIDE	11
1.3 OBJECTIVES	15
2.0 METHODOLOGY	16
2.1 ANALYTICAL WORK	16

2.1.1	LIM THRUST PRODUCTION	16
2.1.2	AIR GAP SIZING	18
2.2	COMPUTER SIMULATION	19
2.2.1	MATLAB/SIMULINK MODEL	19
2.2.2	MATLAB REGRESSION MODEL	23
2.3	EXPERIMENTAL WORK	24
2.3.1	GUIDEWAY/CART TESTING	24
3.0	RESULTS AND DISCUSSION	33
3.1	AIR GAP VARIATION	33
3.2	PITCH ANGLE VARIATION	35
3.3	BANK ANGLE VARIATION	38
3.4	YAW ANGLE VARIATION	40
3.5	TESTING USING WOODEN GUIDEWAY	45
3.5.1	AIR GAP VARIATION	45
3.5.2	BANK ANGLE VARIATION	46
3.5.3	PITCH ANGLE VARIATION	48
3.6	FACTOR SENSITIVITY	49
3.7	ELECTRICAL POWER AND EFFICIENCY	50
3.8	MOTOR SIZING CONSIDERATIONS	53
4.0	CONCLUSIONS AND FUTURE WORK	54
	REFERENCES	56
	APPENDIX A – MOTOR CONFIGURATION CALCULATIONS	58
	APPENDIX B – FORCE ENGINEERING F951 LIM DATASHEET	60
	APPENDIX C – EMERSON UNIDRIVE SP0201 BROCHURE EXCERPT	61

APPENDIX D – ARDUINO SOURCE CODE FOR CURRENT DATA COLLECTION	62
APPENDIX E – ARDUINO SOURCE CODE FOR MOTOR CONTROL	63
APPENDIX F – MATLAB CODE FOR DATA PROCESSING AND PLOTTING	70
APPENDIX G – SAMPLE REGRESSION MODEL COEFFICIENTS	72
APPENDIX H – H2W LMG-06-650-SSE LIM datasheet	73

## **NOMENCLATURE**

AC	alternating current
ATN	automated transit system
Bogie	apparatus including wheels, axles, drive motor(s), and frame that supports the pod car on a track. The car may be mounted above or hung below the bogie.
DC	direct current
emf	electromotive force
LIM	linear induction motor
LSM	linear synchronous motor
Maglev	magnetic levitation
PRT	personal rapid transit

## LIST OF FIGURES

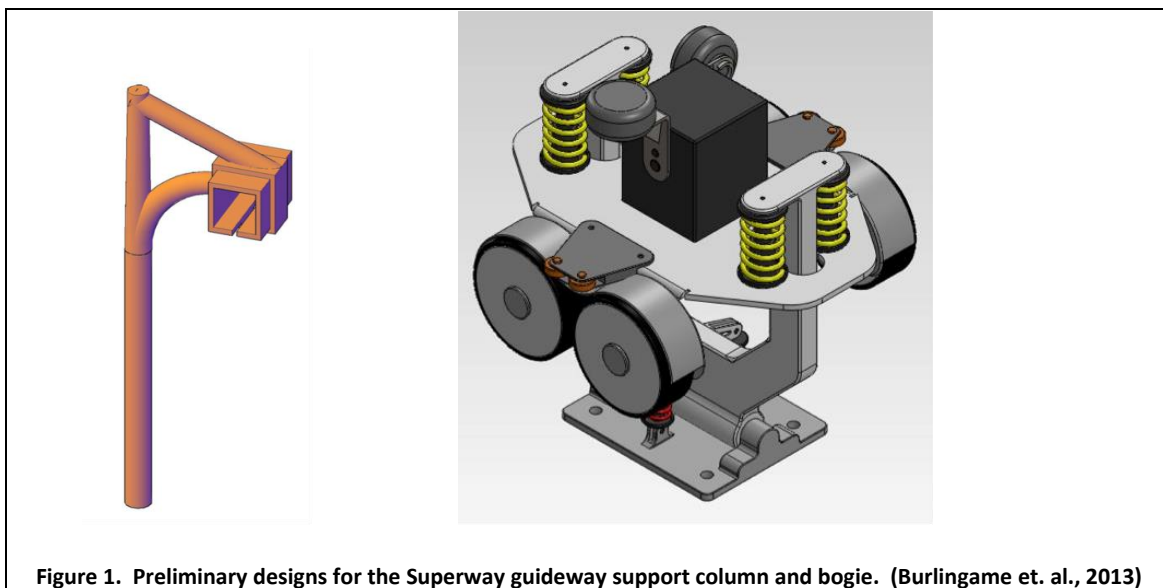
<u>Title</u>	<u>Page</u>
Figure 1. Preliminary designs for the Superway guideway support column and bogie	1
Figure 2. Comparison of a LIM to a rotary induction motor	4
Figure 3. Loss of traction in freezing conditions	6
Figure 4. Maglev train in Shanghai, China	8
Figure 5. Guideway showing long-primary LIM configuration	9
Figure 6. Map of linear motor transit systems	10
Figure 7. Example of a PRT bogie	14
Figure 8. Simplified per-phase model of an induction motor	17
Figure 9. Simulink model of LIM	21
Figure 10. Theoretical LIM acceleration	22
Figure 11. Comparison of observed data to regression model predictions	24
Figure 12. LIM setup from 3D model	25
Figure 13. Closer view of 3D model	26
Figure 14. Front profile view of 3D model	27
Figure 15. Close-up view of the motor guide rail	28
Figure 16. Early circuit used for acceleration data collection	29
Figure 17. Apple iPhone 4 mounted in acrylic frame	30
Figure 18. Linear encoder strip shown with yaw angle variation bogie	31
Figure 19. Alternate bogie and guideway	32
Figure 20. Closed-loop acceleration with variable air gap	34
Figure 21. Averaged closed-loop acceleration with variable air gap	34

Figure 22. Motor current from closed-loop air gap variation	35
Figure 23. Closed-loop acceleration with variable pitch angle	37
Figure 24. Averaged closed-loop acceleration with variable yaw angle	37
Figure 25. Motor current from closed-loop pitch variation	38
Figure 26. Closed-loop acceleration with variable bank angle	38
Figure 27. Averaged closed-loop acceleration with variable bank angle	39
Figure 28. Motor current from closed-loop bank variation	39
Figure 29. Free body diagram of LIM with non-zero yaw angle	40
Figure 30. Closed-loop acceleration with variable yaw angle	41
Figure 31. Averaged closed-loop acceleration with variable yaw angle	41
Figure 32. Motor current from closed-loop yaw variation	42
Figure 33. Open-loop acceleration with variable yaw angle	43
Figure 34. Open-loop averaged acceleration with variable yaw angle	44
Figure 35. Detail view of yaw variation data	44
Figure 36. Comparison of acceleration between bogie/guideway setups	45
Figure 37. Average acceleration vs. air gap for both bogie/guideway setups	46
Figure 38. Acceleration vs. bank angle for both bogie/guideway setups	47
Figure 39. Average acceleration vs. bank angle for both bogie/guideway setups	47
Figure 40. Average acceleration vs. pitch angle for both bogie/guideway setups	48
Figure 41. Average acceleration vs. pitch angle for both bogie/guideway setups	49
Figure 42. Factor sensitivity of LIM output	50
Figure 43. An electrical circuit using delta wiring	51
Figure 44. Efficiency of the LIM under varying air gap size and motor speed	52
Figure 45. Watts of electrical power consumed per newton of force output	53

## 1.0 INTRODUCTION

This paper investigates linear induction motors (LIMs) as the primary propulsion source in a proposed automated transit network (ATN). The network is called Superway, and will be located in the Silicon Valley region near San José, CA. It is being developed by an interdisciplinary group of students and faculty at San José State University (Burlingame, et. al., 2013). This study was motivated by a lack of available research about the behavior of LIMs under less-than-perfect real-world applications with installation misalignments or improper air gap settings.

Superway will use a hollow elevated guideway to carry small vehicles suspended beneath the support structure – wheels, axles, drive motor(s), and frame, collectively referred to as a “bogie” – that rides within the guideway. Each vehicle will seat up to four passengers. At the originating station passengers may request a vehicle or simply alight into one that is already



waiting. Once a destination has been selected, service is point-to-point with no intermediate stops because stations are located off of the main line of travel, allowing vehicles to bypass all

but the intended destination station. The central control system will select the fastest path from origin to destination based on current system traffic delays or other issues.

Each pod will need to vary its acceleration and speed in order to comply with directives from the central control system. Much like an automobile traveling on a freeway, it will be required to increase or decrease speed in response to its immediate surroundings. Control inputs will include the presence of hills, curves, merge areas, and other traffic ahead or behind.

I have a long-held interest in transportation not based on the internal combustion gasoline engine, and was happy to accept when invited to participate in this project.

What follows is an overview of modern LIM technology and important design criteria. Other propulsion motor options are also considered.

## **1.1 Literature Review**

### **1.1.1 Background**

Electric motors produce forces through the interaction of electrical current flowing through an area of magnetic flux. The physics of this interaction have been studied since the early 1800s (Ampere, 1827), and are quite well understood.

Magnetic flux may be produced either by permanent magnets or by passing current through a coil (or coils) of wire surrounding a core of magnetically permeable material, forming an electromagnet.

If mechanically constrained to move in rotation only, these forces become a torque exerted between the stationary frame of the motor (stator) and the rotating component (rotor). Normally the rotor is connected to an output shaft either directly or through an integrated gearbox, and this output shaft provides torque for the desired application of the motor.

### **1.1.2 DC Machines**

There have been many different types of electric motors throughout the years. Simple direct current (DC) machines use permanent magnets fixed to the stator to produce flux. They incorporate several rotor windings wired to a commutator, and use carbon brushes to transmit DC current to the particular rotor winding with the optimal orientation for a given rotor position to produce the greatest torque (Wildi, 2002). However brushes are high wear items requiring frequent replacement, and the constant on-off action of the inductive winding coils causes arcing that emits high levels of electromagnetic noise and acts as an ignition source, making such motors impractical or unusable in many situations.

### **1.1.3 Synchronous AC Machines**

Some of these issues may be solved by swapping components between stator and rotor, i.e. using permanent magnets in the rotor and controlling the current through windings in the stator. This configuration eliminates the need to transmit power to the rotor, but requires accurate information about rotor position in order to determine the proper timing of the stator current. These are called permanent magnet synchronous alternating current (AC) machines. Simply applying a DC voltage will no longer cause continuous rotation, but rather will cause the rotor to orient to a particular angle and then stay fixed. An alternating current input is now required for continuous rotation, and it is the frequency of this AC signal that determines the steady-state speed of the machine (Hsu, 2013).

### **1.1.4 Induction Machines**

In an induction motor design, the rotor windings are not accessible from the outside of the motor, but rather are shorted together internally. Only the stator windings are controllable.

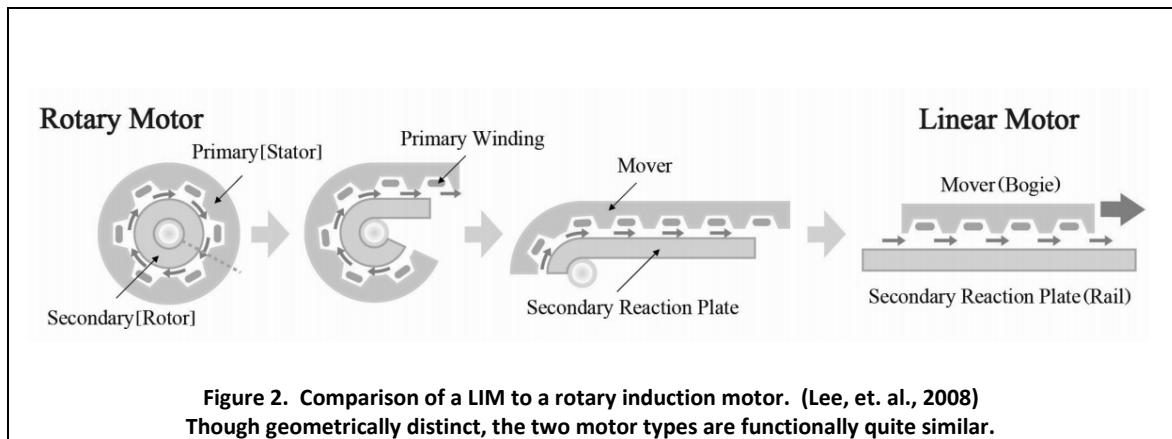
AC power is supplied to the stator windings, creating varying lines of flux that cross the rotor. This induces current in the rotor windings, and it is this induced rotor current interacting with the stator flux that produces torque (Hsu, 2013).

In order for appropriate stator inputs to be applied, accurate information is needed about the instantaneous values of rotor position, rotor speed, rotor current, rotor flux, stator current, and stator flux. Some of these values (stator current and flux, rotor position and speed) may be measured directly while others (rotor current and flux) must be estimated or calculated from measured or otherwise known values. It was the advent of high-speed, low-cost microcontrollers that allowed the widespread use of induction motors by enabling these calculations in real time.

### 1.1.5 Linear Induction Machines

It was mentioned earlier that these electric machines must be mechanically constrained to only rotate in order to produce the torque that we normally associate with a motor. But one may ask, “What happens if a machine is not constrained as described?”

If one can imagine taking a standard rotational induction machine, cutting it along a radius, and unwinding it to a flattened shape, the result is a linear induction motor.



The electrical construction is identical, only now the motion is no longer constrained to be rotational only. Whereas before the parts of the machine were referred to as a controllable *stator* and a passive *rotor*, the designations now become the controllable *primary* and the passive *secondary*. In practice, the secondary usually consists of a simple aluminum plate with a steel backing plate (Gastli, 2013). The aluminum is selected for its low electrical resistivity<sup>1</sup>, while the steel acts as a strengthening support and flux return path.

Current is passed through the primary windings, producing flux that then induces eddy currents in the secondary plate. These eddy currents interact with the magnetic field from the primary, producing a both a lateral force and a normal force between primary and secondary.

There are two distinct types of LIM implementations:

- Short primary, where the powered “stator” coils are attached to the vehicle and act on a stationary reaction plate, and
- Long primary, where the vehicle carries the reaction plate and the motors are mounted in the track or guideway.

### **1.1.5.1 Advantages Over Rotary Machines**

Several performance improvements are realized through the use of a linear motor. The longitudinal force produced by a LIM is used to directly drive a vehicle along a track or guideway. This is in contrast with a rotary machine that must drive a gearbox, driveshaft, or axle, which then converts the output torque to a frictional force between the wheels and the supporting surface. By using a LIM, mechanical losses from these power transfer devices are

---

<sup>1</sup> Some railway applications have attempted to use the iron railway guide rails as the secondary, but the higher resistivity of iron vs. aluminum was very detrimental to performance (Binder, et. al., 2001).

eliminated. This can yield a power savings of 5% or more (California Energy Commission, 2013). Operation is also quieter and requires far less maintenance.

Perhaps more significantly, vehicle acceleration – both forward thrust and electric braking – become independent of friction between the wheels and the surface. The most obvious benefit of this fact is that vehicle performance is largely unaffected by rain, snow, ice, sand, or other environmental contaminants on the travel surface (Vectus, 2013). The vehicle is also able to safely climb steeper grades. Design considerations that were once compromised between efficiency and traction can now be made to minimize frictional forces and rolling resistance. This development even permits the removal of wheels altogether, in the case of magnetic levitation – or maglev – applications.



**Figure 3. Loss of traction in freezing conditions.**  
Traditional wheeled vehicles depend on friction between driven wheels and the supporting surface. If contaminated with snow or ice, such drivetrains may become unusable. (Daily Courier, 2013)

Under normal use conditions, LIMs have no moving parts; they require no periodic maintenance such as lubrication or replacement of seals or other soft parts.

Certain situations, such as very massive vehicles travelling on steep grades, necessitate large thrust forces and correspondingly high power output. Heat transfer devices such as water-

cooled plates or simple passive heat sinks may be employed to prevent drive components from overheating. Such measures can increase cooling capacity considerably, up to six times more effective than passive air-cooling (Force Engineering, 2013). However, given the flat terrain in Silicon Valley such additional equipment would likely not be necessary.

### **1.1.5.2 Disadvantages**

The electrical efficiency of LIMs tends to be considerably lower – sometimes as much as 40% – when compared directly to a rotary machine (Fazel, et. al., 2012). This is due to energy lost to end effects, where flux produced by the primary is prone to leakage at the exit end without performing any useful work. Rotary motors do not experience these losses because of the nature of their continuous-loop topology. However such direct comparisons often neglect the other components required to convert an output torque into linear motion. As mentioned earlier, power transfer losses can cost 5% or more of drivetrain power. Using a LIM would avoid these mechanical losses.

### **1.1.5.3 Air Gap Considerations**

In rotary motors the air gap between rotor and stator can be kept very small (~1 mm) because it is relatively simple to manufacture the bearings and motor case to tight tolerances, and assemble them with very good collinearity. With a LIM there are many components that can affect the air gap, including wheel diameter and defects, distortion of the bogie, guideway flexure, vehicle path curvature, payload mass, etc. All these factors have allowable tolerances that can add up to require a sizeable nominal air gap in order to prevent collisions between the primary and secondary as the pod moves along the guideway. Typical air gaps for LIMs in transit

service range from about 8 mm up to more than 20 mm (Hellinger, 2009). This larger air gap is the main aggravator of end effects and flux leakage contributing to lower efficiency.

There have been studies that attempt to dynamically control the size of the air gap in order to optimize LIM performance (Park, et. al., 2008). Such systems have been shown to be effective, but also add complexity, bulk, and increased cost to the system.

LIMs can produce a sizeable normal force in addition to longitudinal thrust (Park, et. al., 2008). This normal force scales in inverse proportion to the cube of the air gap, while thrust scales inversely proportional to the square of the air gap. Depending on the system geometry and the orientation of a LIM relative to its secondary, this normal force can add or remove considerable friction and rolling resistance loads.

This normal force is frequently used to suspend the vehicle in maglev applications. A portion of the vehicle structure can be extended around the edge and underneath the guideway, locating the primary beneath a bottom-mounted secondary. Alternatively, permanent magnets may be used to produce the majority of the force required to suspend the vehicle. Controllable electromagnets are then used to carefully adjust the total flux so that the vehicle's distance from the guideway is kept constant.



**Figure 4. Maglev train in Shanghai, China.**

**This train must use linear motors because it has no contact with the guideway. (Burlingame, et. al., 2013)**

## 1.2 Operational Systems Worldwide

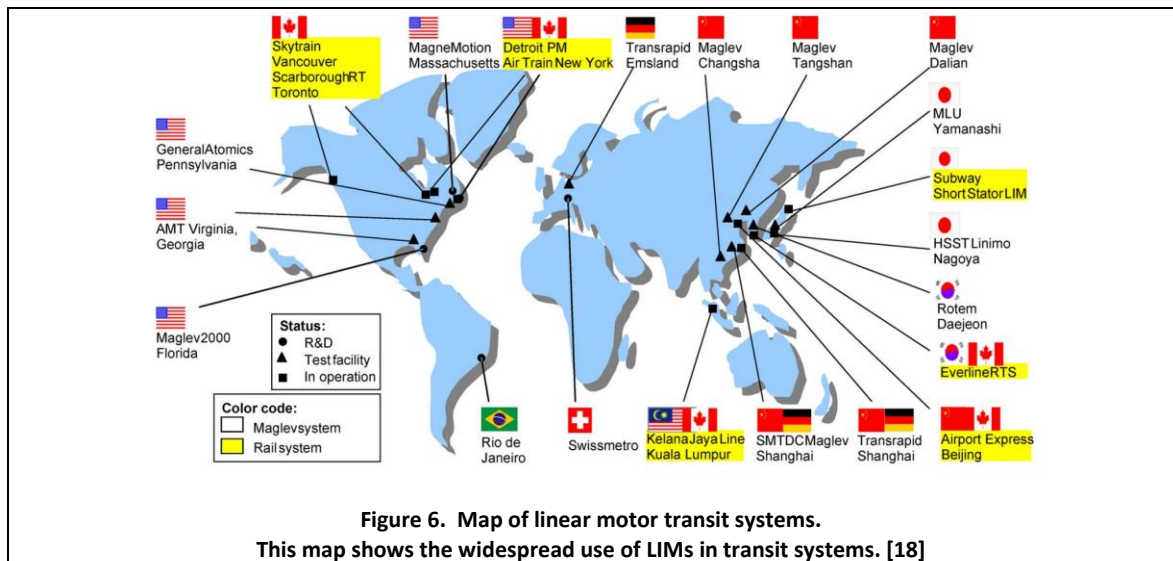
### 1.2.1 Transit Systems Using LIM Propulsion

Looking at transit systems employing LIMs worldwide, the decision to use a short primary versus a long primary has depended largely on the intended speed of the application. Most systems using speeds up to about 100 km/h opt for a short primary, while those above that threshold generally select a long primary because the transfer of power to the vehicle becomes more problematic as speed increases.



Figure 6 and Table 1 show several LIM-powered transit systems around the globe.

The two high-speed maglev trains (Shanghai and Yamanashi) each use a long primary linear synchronous motor (LSM). The long primary configuration allows the propulsion coils to receive power from stationary supply lines, eliminating any physical connection to the vehicles. The synchronous motors require more precise location sensing, but power requirements increase dramatically with aerodynamic drag at such high speeds (500 km/h +), making the less-efficient LIM far less practical.



As shown in Table 1, those transit systems currently using a LIM for propulsion are overwhelmingly using a short primary motor attached to the vehicle and a reaction plate mounted to the track or guideway. These are full-size railcars traveling on tracks sized for conventional rail – they generally employ longer and wider vehicles that leave the form factor of the motor unconstrained in size. That is, they have plenty of room for several motor primaries per vehicle, allowing more motors and thus a reduction in the size or duty cycle of individual motors while still being able to produce the required thrust.

In the case of a smaller PRT vehicle suspended from a size-constrained bogie, space comes at much more of a premium. The thrust required for acceptable performance of our PRT system is easy to quantify, but constructing a compact LIM that can provide that thrust is a different matter.

Table 1: Worldwide transit systems using linear motor propulsion.

Name	Location	Motor Style	Drive / Support Material	Currently in Operation?
Skytrain	Vancouver, Canada Group light rail	LIM (Bombardier ART short primary)	Steel/steel	Yes
3 Scarborough SRT	Toronto, Ontario, Canada	LIM (Bombardier ART short primary)	Steel/steel	Yes
AirTrain JFK	New York, NY	LIM (Bombardier ART short primary)	Steel/steel	Yes
Kelana Jaya Line	Kuala Lumpur, Malaysia	LIM (Bombardier ART short primary)	Steel/steel	Yes
Airport Express	Beijing, China	LIM (Bombardier ART short primary)	Steel/steel	Yes
EverLine	Yongin, South Korea	LIM (Bombardier ART short primary)	Steel/steel	Yes
Toei Ōedo Line	Tokyo, Japan	LIM short primary	Steel/steel	Yes
Green Line	Yokohama, Japan	LIM short primary	Steel/steel	Yes
Kaigan Line	Kobe, Japan	LIM short primary	Steel/steel	Yes
Moscow Monorail	Moscow, Russia	LIM short primary	Steel/steel	Yes
Nanakuma Line	Fukuoka, Japan	LIM short primary	Steel/steel	Yes
Rapid Electric Tramway Ln. No. 7	Osaka, Japan	LIM short primary	Steel/steel	Yes
Yamanashi Maglev Test Line	Tsuru, Japan	LSM long primary	Maglev/rubber/ concrete	Testing
Shanghai Maglev Train	Shanghai, China	LSM Transrapid long primary	Maglev	Yes
Magnetbahn	Berlin, Germany	LSM long primary	Partial maglev/ steel/steel	No (1991)
Linimo HSST	Nagoya, Japan	LIM short primary	Maglev	Yes

## 1.2.2 PRT Systems Worldwide

There are only a few successful PRT systems around the world that have actually been built and have become operational. They are briefly described in Table 2.

The reasons for selecting a LIM over a more conventional rotary motor usually can be narrowed down to two: the independence of thrust from surface friction, and the low maintenance requirements of zero moving parts. However, as can be seen above in Table 2, the decision to use a LIM is by no means universal. In fact, there are no PRT systems currently operating that use LIMs as the primary propulsion source.

**Table 2. Developed PRT Systems Around the World**

<b>Name</b>	<b>Location</b>	<b>Motor Type</b>	<b>Drive / Support Material</b>	<b>Currently in Operation?</b>
ULTra Global PRT	London, Heathrow Airport	Rotary	Rubber/concrete	Yes
ULTra Global PRT	Amritsar, India	Rotary	Rubber/concrete	Construction stalled
SkyCube (Vectus)	Suncheon Bay, South Korea	Rotary	Steel/steel	Yes
WVU PRT	West Virginia University, Morgantown WV	Rotary	Rubber/concrete	Yes
2getthere	Masdar City, UAE	Rotary	Rubber/ concrete	Limited
Cabintaxi	Hagen, Germany	Double DSLIM short primary	Steel/steel	No (1979)

One recognizes several important characteristics of a LIM required in a PRT system: performance specifications determine the required thrust. To achieve the required thrust there are two basic degrees of freedom: available instantaneous thrust and motor duty cycle. These two factors are constrained by two others: physical size, and (naturally) cost.

The goal becomes, then, to select a motor that 1) meets the performance criteria, 2) fits within the physical limitations of the system, 3) has the lowest cost.

The performance metrics are largely determined by human factors, namely the maximum longitudinal acceleration tolerable to the average passenger. Studies have been conducted regarding these limits (Hoberock, 1977) and 0.14 g has been found to be a reasonable value for a seated passenger. Another important factor is jerk, or the rate of change of acceleration. Jerk limits are generally kept below 0.3 g/second, or about 2.9 m/s<sup>3</sup>. Perhaps

counterintuitively, a standing passenger is generally more tolerant of higher levels of acceleration and jerk than a seated passenger.

Based on a starting vehicle mass of 1133 kg, the required thrust is in the range of 1.6-2.5 kN, depending of the additional mass of the propulsion system attached to the vehicle.

Calculations for determining these values may be found in the appendix. If a short primary topology is used, the vehicle will need to carry more mass (battery/power transfer equipment, power electronics, LIM), whereas if the motors are mounted in the guideway in a long primary configuration, the vehicle needs to carry only a reaction plate.

This impact of this design point cannot be overstated. With the short primary, the guideway is simplified at the cost of a more complex and therefore massive vehicle. This generally results in much lower construction costs as the number of vehicles determines the required number of LIMs, rather than the total length of guideway in the system. However, motor efficiencies tend to be far lower (as much as 70% lower than long primary) due to adverse end effects and flux leakage (Wu, et. al., 2010). This increased energy consumption contributes to higher operating costs. Also, the LIM in the vehicle must be able to operate at nearly a 100% duty cycle and must be sized for the most demanding conditions in the system, requiring a more robust (i.e. large and heavy) design.

The long primary keeps the vehicle and its systems much simpler, as propulsion equipment is located in the guideway instead. Thus the need to supply propulsion power to the vehicle through battery packs, a third rail, or a power induction circuit is removed. The resulting vehicle is smaller, lighter, and cheaper. The guideway becomes far more expensive, however. In order to prevent pulsating thrust variations and ensure positive control at all times, the maximum motor pitch is limited to the length of the vehicle support structure, or bogie, to which the secondary plate is attached, and is often only half of this length. Assuming a 1.5m

motor pitch, even a modestly sized system will require thousands of LIMs, compared to perhaps a few hundred for a short primary system. On the other hand, each motor is only in use while a vehicle is passing by it, resulting in duty cycles generally below 5% and a corresponding reduction in required robustness, cooling equipment, and cost per motor.



**Figure 7. Example of a PRT bogie. This image shows several common components of a bogie- support wheels, structural frame, guide wheels, and center-mounted secondary. (Kable, 2014)**

The up-front construction costs involved with a long primary configuration make it a very hard sell to public agencies and private financiers alike. Performance considerations and operating costs certainly favor the long primary, but it requires the purchase and installation of about ten times as many LIMs, even if they are mostly reduced in size compared to the short primary topology.

Rotary motors can be an attractive lower-cost alternative, but are likely not available in a small enough form factor to supply main propulsion and still fit inside the guideway currently

proposed by the Superway team. Given that a visually unobtrusive guideway is a strong focus of the design, this is likely a disqualifying factor. A rotary motor can also add a hundred kilograms or more to the mass of the vehicle, significantly impacting performance and leading to a repeating, incremental loop of increasing mass requiring more torque requiring a more massive motor requiring even more torque...

Note from Table 2 that the only PRT system built to date that has used a short primary LIM was the Cabintaxi system (Cabintaxi, 2012). It used two sets of dual-sided LIMs- essentially four LIM units all mounted inside the same guideway. It is expected that a similar configuration may be required in order to meet the performance specifications for the Superway system. Additionally, if the LIM primaries are mounted below the secondary plate, the attractive normal force will serve to remove some weight from the main bogie wheels, improving overall efficiency.

There are several advantages to LIMs that contributed to the team's decision to consider them for the Superway application: they are able to meet the basic thrust demands of the system, and they are contactless without any moving parts.

If a short primary design is selected, locations that require more thrust, such as station exits and areas approaching a merge, can receive higher-output motors to satisfy local acceleration needs without adding unnecessary capacity everywhere in the system.

### **1.3 Objectives**

Traditionally, LIM are put into service under controllable conditions, generally indoors, protected from the elements, and easily accessed for service. In the case of Superway, motor placement would be in relatively unfriendly environments, subject to conditions such as condensation, vibration, seasonal and daily temperature variations, and the like. Their

mounting location inside an elevated guideway will make it unlikely that vandals will target them, but it also poses challenges for service access.

Much attention has been given to LIM performance, but few studies could be located that addressed the fault tolerance of LIMs. We know that a LIM in good working order will meet the needs of Superway, but what happens when things begin to go awry, and the Department of Public Works has a backlog of work orders? Will the entire Superway system grind to a halt, or will a LIM be able to perform adequately in the interval of days or weeks between fault occurrence and a service call?

The Superway team has decided to study the use a LIM-based propulsion system, but much of the detail design has yet to be finalized. The task addressed by this project is the categorization of a LIM operating under less-than-ideal conditions to help determine if LIM behavior is robust enough for an application as safety-critical as Superway or other, similar ATNs.

## **2.0 METHODOLOGY**

### **2.1 Analytical Work**

#### **2.1.1 LIM thrust production**

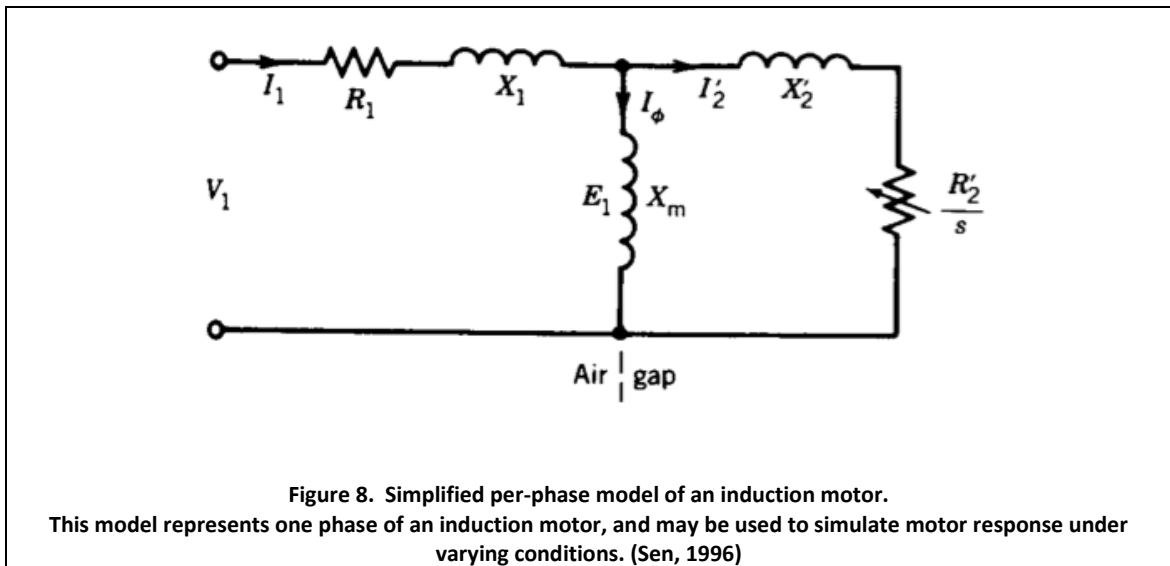
In a rotary induction motor, a voltage difference is applied across the three-phase stator windings in sequence to produce a rotating flux field. This. The difference in speed between the rotor and the flux field is called slip, defined as:

$$S = \left(1 - \frac{\dot{\theta}}{\omega_s}\right) \tag{1}$$

where  $\dot{\theta}$  is the speed of the rotor, and  $\omega_s$  is the rotational speed of the flux field. If slip is not zero, the rotating flux field crosses the windings in the rotor, inducing currents. These currents then experience a Lorentz force as they interact with the flux field, thus applying torque to the motor shaft. The torque equation is the vector cross product of the rotor flux and the stator current:

$$\tau = \psi_r \times I_s = (L_m I_r^s)(I_s) \sin \theta \quad (2)$$

Each of the three motor phases can be considered separately, represented by the simplified circuit shown below in Figure 8. The stator and rotor are each modeled as a resistive element (the resistance of coil windings) in series with an inductive element (the leakage inductance). In series with both of these is a third inductive element, referred to as the mutual inductance. Leakage inductances are generally about 5% of the mutual inductance. (Hsu, *Induction Machines*, 2013) The rotor circuit also shows a voltage source that represents an opposing electromotive force (emf) arising from the reluctance of the rotor.



A linear induction motor is modeled in much the same fashion. The rotor windings are replaced by the secondary reactance plate but the electrical behavior is similar. Rather than a rotating flux, the primary coils produce a translating flux field that travels along the direction of

motion. Instead of applying a torque, the motor delivers a linear force developed by the Lorentz interaction of slip-induced currents in the secondary with the translating primary flux.

The synchronous speed of the LIM is equal to the product of the input voltage frequency and the pole pitch – the distance between consecutive coils of any given phase – of the motor.

## 2.1.2 Air Gap Sizing Considerations

The size of the air gap between primary and secondary determines the flux field density and ultimately the thrust produced by the motor. We know from Equation 2, above, that motor output varies directly with secondary current. This secondary phase current can be expressed this way:

$$I_2 = \frac{I_1}{\sqrt{\frac{1}{(SG)^2} + 1}} \quad (3)$$

where  $I_1$  is the primary current,  $S$  is slip, and  $G$  is goodness factor of the motor, defined thus:

$$G = \frac{2\mu_0 f \tau^2}{\pi \left(\frac{\rho_r}{d}\right) g_e} \quad (4)$$

$\mu$  = permeability of free space (H/m)

$f$  = frequency (Hz)

$\tau$  = pole pitch (m)

$\rho_r$  = volume resistivity of secondary plate ( $\Omega$ -m)

$d$  = thickness of secondary plate (m)

$g_e$  = equivalent air gap

The overall influence of air gap on thrust will vary depending on operating conditions, but it can be seen from the equations above that a larger air gap results in a lower overall thrust. Thus it is in the interest of designers to keep the gap as small as practicable. Unfortunately, in the case of an ATN, maintaining a specific gap can be tricky, as the air gap is the sum of stacked

tolerances of several system components: secondary thickness, steel backing plate thickness, guideway uniformity, wheel roundness and wear, bearing play... Ultimately the system must be designed with a large enough gap to accommodate the worst case of all these tolerance stack-ups while avoiding collisions between primary and secondary.

Tighter tolerances come with a corresponding increase in fabrication, construction, and maintenance costs. Once again we must find an optimal balance between required performance and the financial resources required to achieve it.

## 2.2 Computer Simulation

### 2.2.1 Simulink Simulation Model

A simulation model was built in Simulink using equation 5 (Hsu, 2013). This is a differential equation in matrix form expressed in the stator (primary) frame, using stator and rotor (primary and secondary) voltages as the state variables. It represents a two-phase (x-y) model; we must convert our three-phase (a-b-c) inputs to equivalent two-phase values before applying them, then convert outputs back to three-phase, where applicable.

$$\begin{bmatrix} \dot{I}_{sx} \\ \dot{I}_{sy} \\ \dot{I}_{rx}^s \\ \dot{I}_{ry}^s \end{bmatrix} = \begin{bmatrix} L_s & 0 & L_m & 0 \\ 0 & L_s & 0 & L_m \\ L_m & 0 & L_r & 0 \\ 0 & L_m & 0 & L_r \end{bmatrix}^{-1} \left\{ \begin{bmatrix} v_{sx} \\ v_{sy} \\ v_{rx}^s \\ v_{ry}^s \end{bmatrix} - \begin{bmatrix} R_s I_{sx} \\ R_s I_{sy} \\ R_r I_{rx}^s + \dot{\theta} \psi_{ry}^s \\ R_r I_{ry}^s - \dot{\theta} \psi_{rx}^s \end{bmatrix} \right\} \quad (5)$$

$\dot{I}_{sx}$  = time derivative of primary current in the x-direction

$\dot{I}_{sy}$  = time derivative of primary current in the y-direction

$\dot{I}_{rx}^s$  = time derivative of secondary current in the x-direction, expressed in the primary reference frame

$\dot{I}_{ry}^s$  = time derivative of secondary current in the y-direction, expressed in the primary reference frame

$L_s$  = self-inductance of the primary

$L_r$  = self-inductance of the secondary

$L_m$  = mutual inductance between primary and secondary

$v_{sx}$  = voltage across the primary in the x-direction

$v_{sy}$  = voltage across the primary in the y-direction

$v_{rx}^s$  = voltage across the secondary in the x-direction, expressed in the primary reference frame

$v_{ry}^s$  = voltage across the secondary in the y-direction, expressed in the primary reference frame

$R_s$  = resistance of the primary

$R_r$  = resistance of the secondary

$I_{sx}$  = primary current in the x-direction

$I_{sy}$  = primary current in the y-direction

$I_{rx}^s$  = secondary current in the x-direction, expressed in the primary reference frame

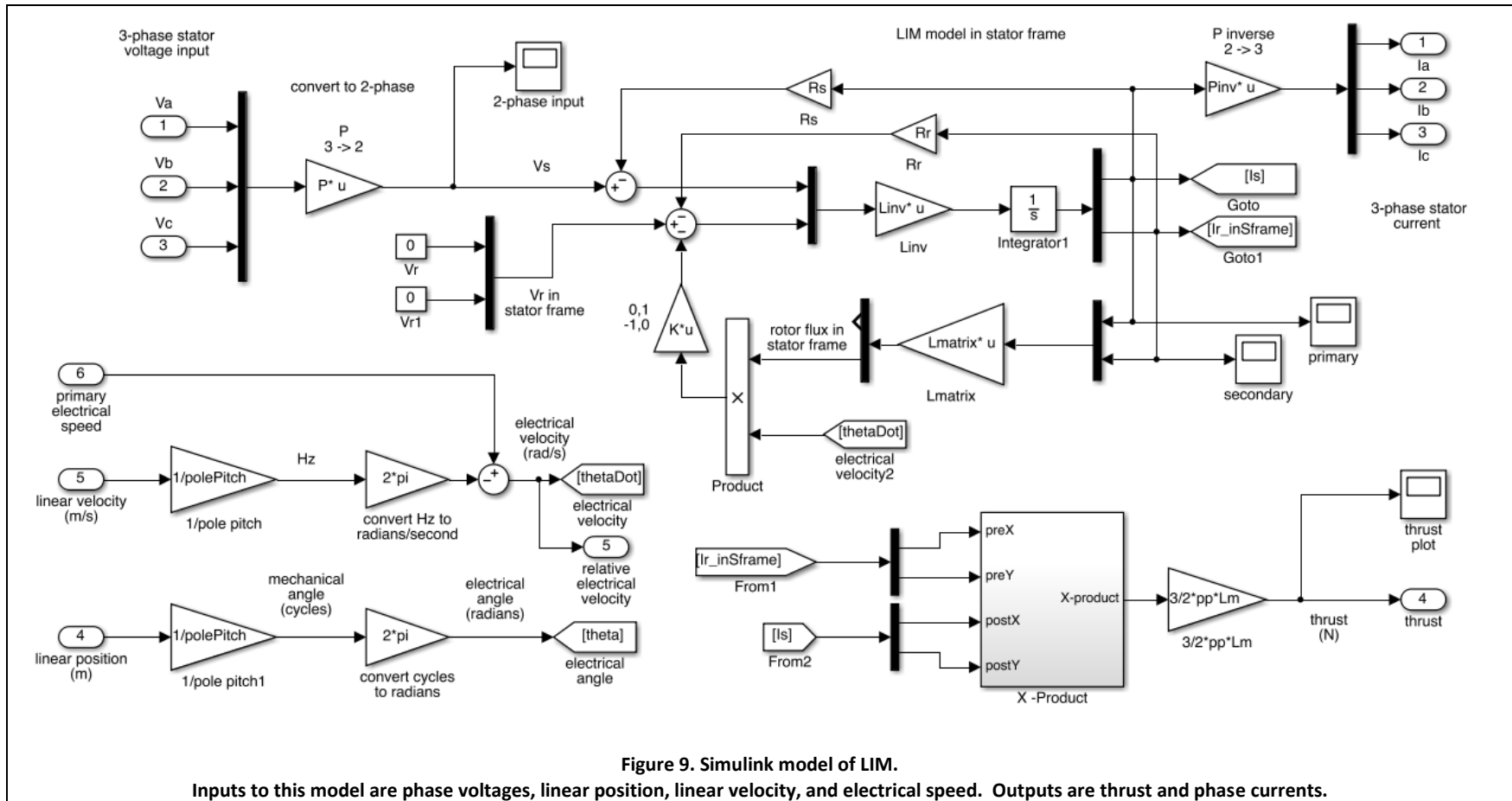
$I_{ry}^s$  = secondary current in the y-direction, expressed in the primary reference frame

$\psi_{rx}^s$  = secondary flux in the x-direction, expressed in the primary reference frame

$\psi_{ry}^s$  = secondary flux in the y-direction, expressed in the primary reference frame

$\dot{\theta}$  = time derivative of the electrical angle

The Simulink model is shown in Figure 9. Simulations were conducted to determine the expected thrust output for the various LIM configurations.



Once the primary and secondary currents are calculated, they are used along with the mutual inductance to determine the thrust output using equation 6.

$$Thrust = (I_r^s \times I_s) \left( \frac{3}{2} L_m \right) \left( \frac{\#of\ poles}{2} \right) \quad (6)$$

$I_r^s$  = secondary current expressed in the primary frame

$I_s$  = primary current

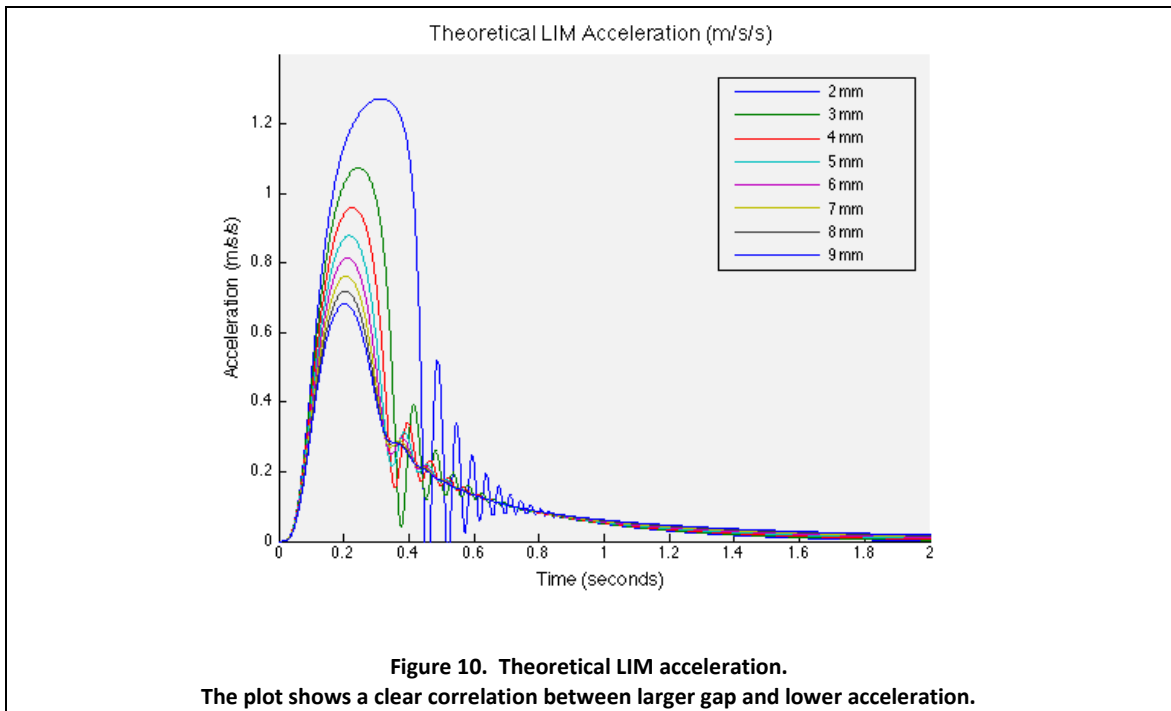
$L_m$  = mutual inductance between primary and secondary

where the mutual inductance may be estimated by:

$$L_m = \frac{k_{Lm}}{\sqrt{g_m}} \quad (7)$$

$k_{Lm}$  = motor geometry coefficient

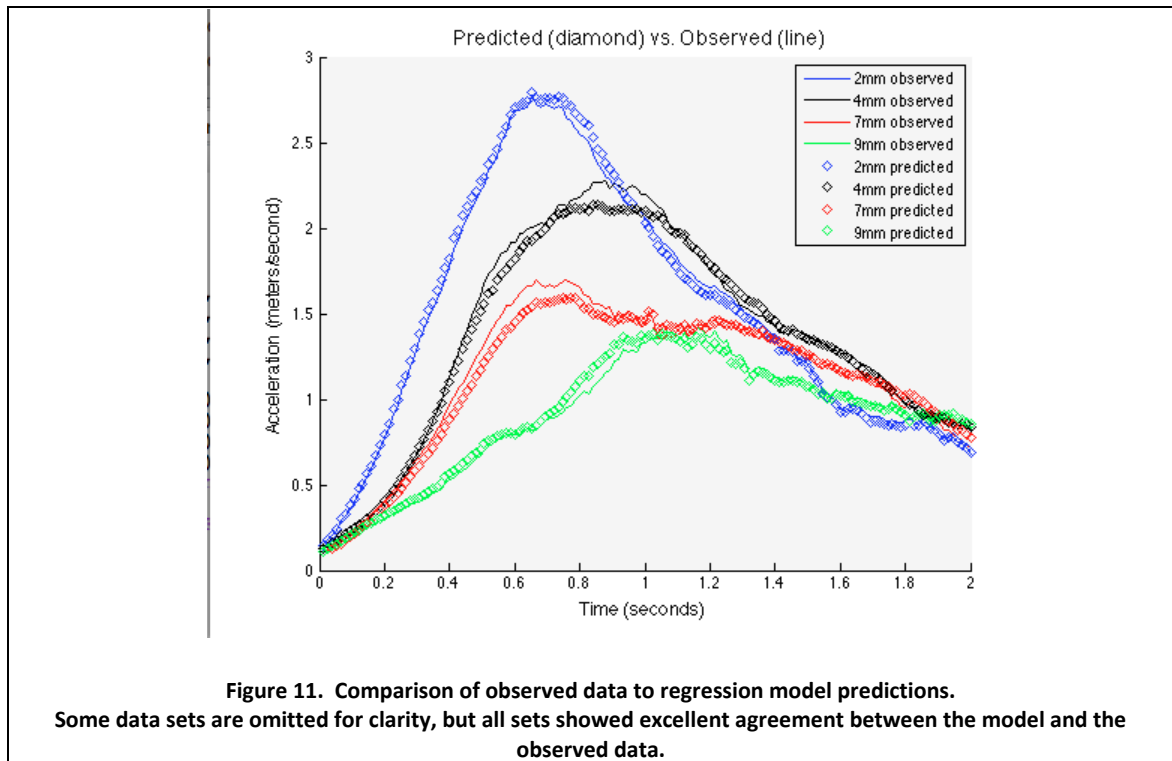
$g_m$  = air gap (millimeters)



### **2.2.2 MATLAB Regression Model**

In order to create an accurate model of the LIM, certain electromagnetic parameters (mutual inductance, stator and rotor resistance and inductance, friction losses) must be known, calculated, or assumed. Force Engineering has been unwilling to share any details about the motor's construction, so these values must be discovered using other methods. There exists a procedure for rotary induction motors that makes measuring the resistance and inductance of stator and rotor coils straightforward. However, because it involves running the motor under a no-load condition while taking measurements, it is problematic to apply the same methods to a linear induction motor with a limited range of motion. Therefore rather than measuring these parameters, data was gathered from the experimental setup and a regression model was developed that adequately reproduced the response of the physical motor.

The model uses a series of third-degree polynomials to calculate the expected acceleration for a given time point using only the size of the air gap as an input. A sample of the coefficients of these polynomials may be found in Appendix G. A comparison of the model results to experimental data is shown below in Figure 11.



## 2.3 Experimental Work

### 2.3.1 Guideway/Cart Testing

A model F951 LIM was acquired from Force Engineering of Leicestershire, UK. While this motor is certainly not powerful enough to be useful in the Superway application, it nonetheless serves to provide data that should scale to larger motors that are more appropriate for the full-size system.

To control the motor, an Emerson SP0201 variable-frequency drive (VFD) three-phase motor controller was selected. The Emerson unit is a full-featured VFD, allowing custom settings for hundreds of control parameters.

A test apparatus was built to support the LIM, as detailed in Figures 12-14. The sliding chassis consisted of an aluminum plate, two steel ball linear bearings, and a single wheel with

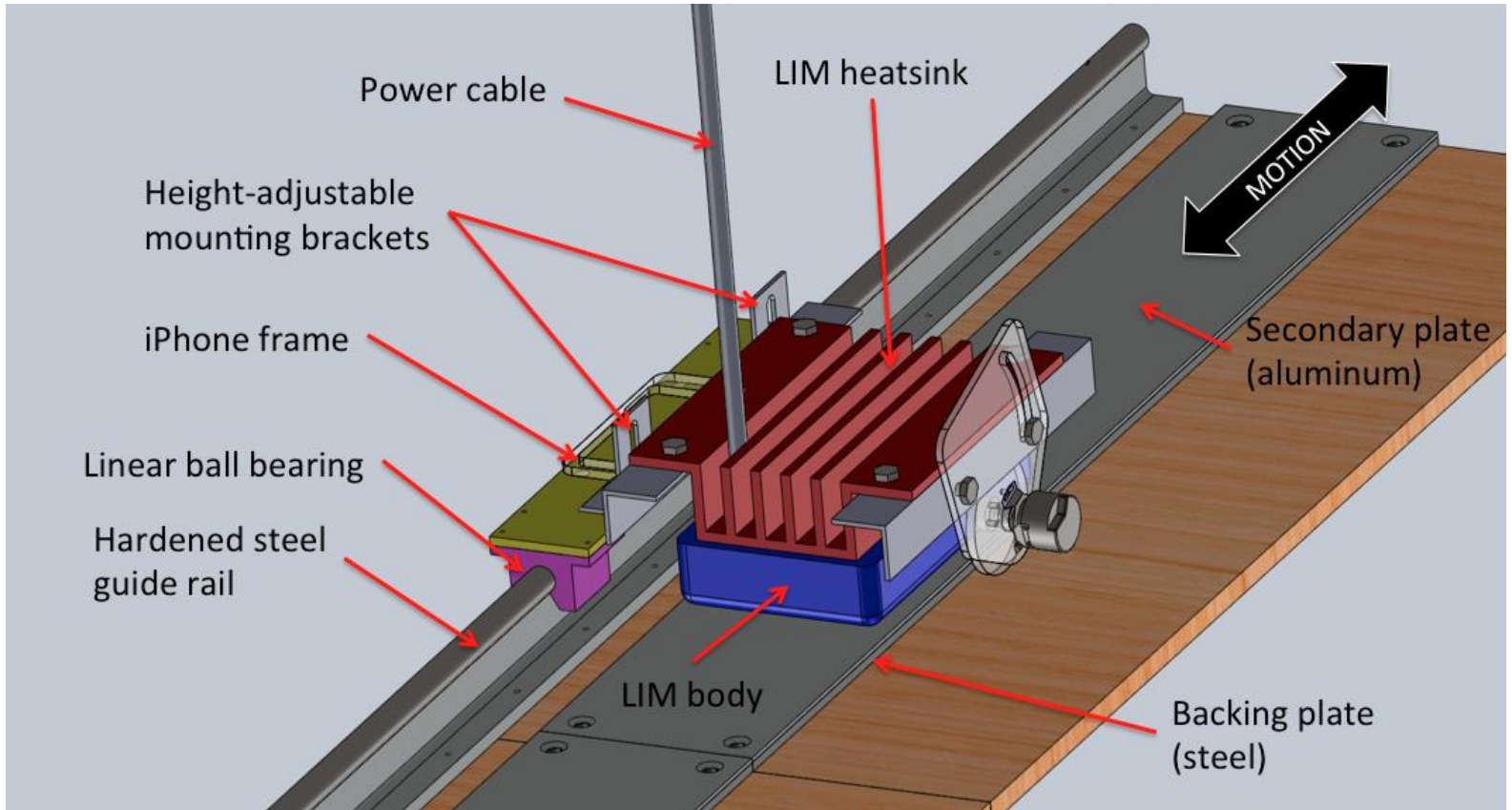


Figure 12. LIM setup from 3D model.

This shows the final configuration, using the iPhone for an accelerometer and the rotary encoder for position feedback.

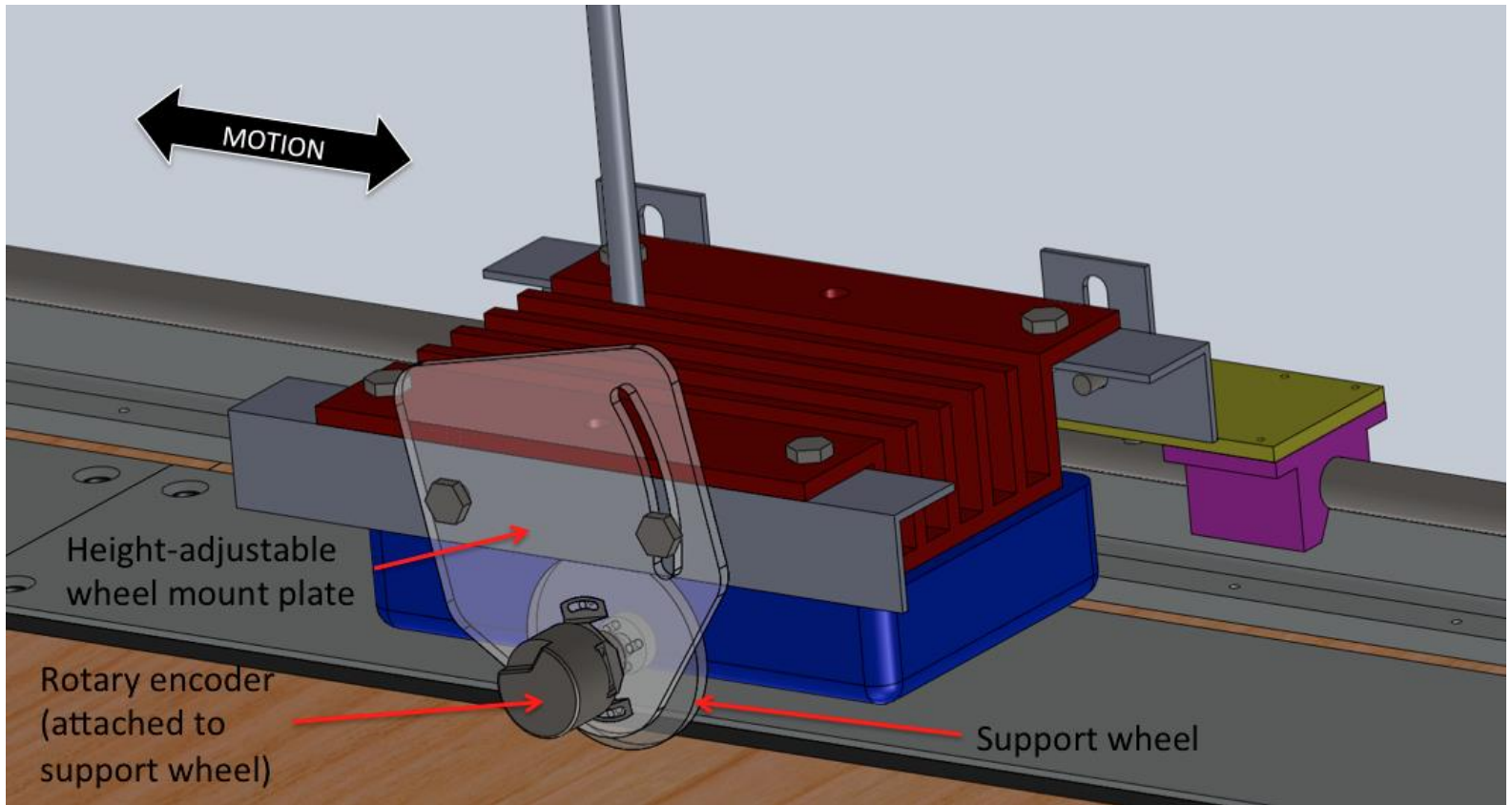


Figure 13. Closer view of 3D model.

The rotary encoder is shown as attached to the support wheel. The height is adjustable for setting air gap and bank angle.

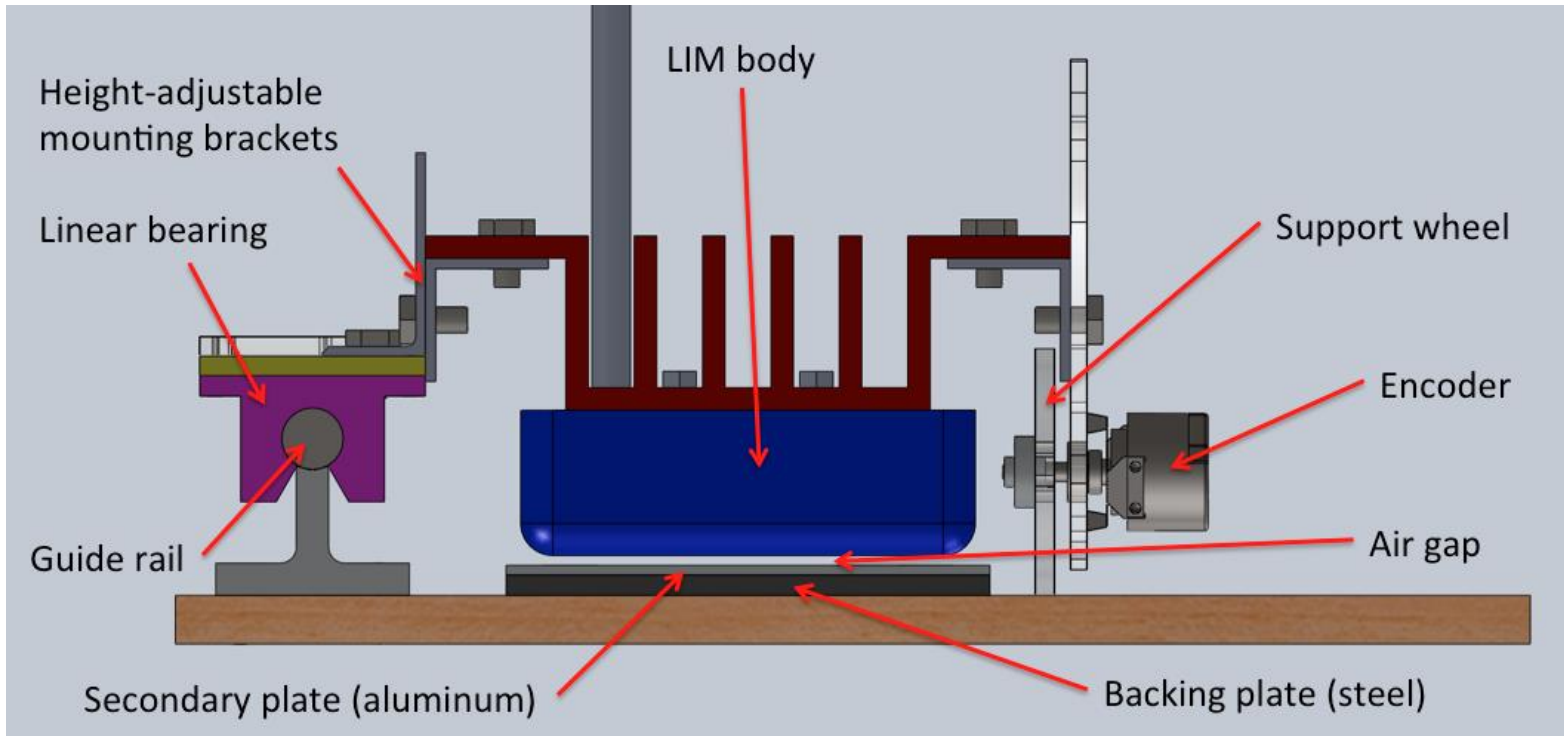
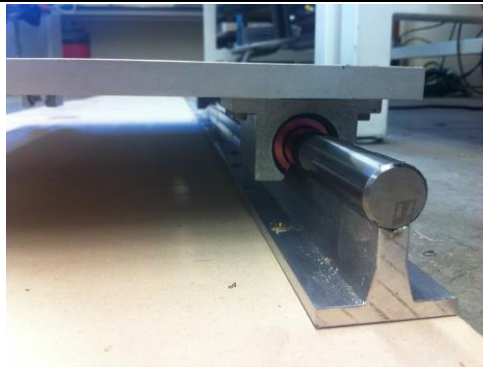


Figure 14. Front profile view of 3D model.  
This view shows the air gap under the LIM body.

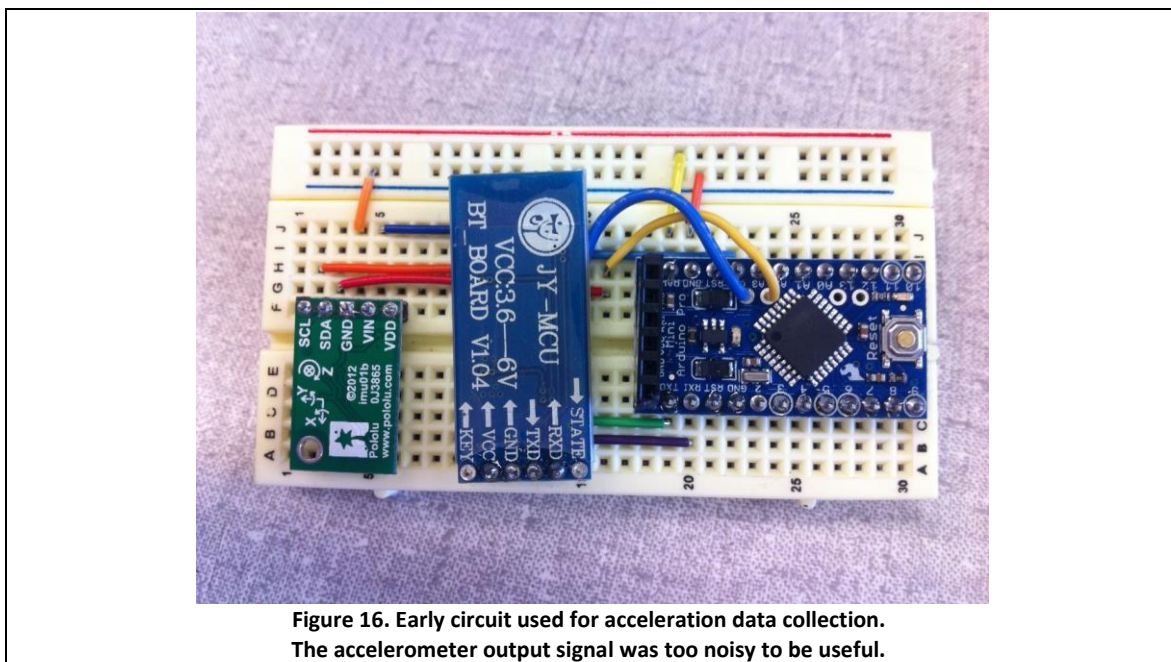
attached rotary encoder. Adjustable mounts allowed for the precise setting of LIM height, pitch, and roll angles. The mass of the bogie, motor, and sensors was 10.17 kg. Variation of the yaw angle was accomplished using a special backing plate with mounting holes for the motor at intervals of five degrees of rotation; this configuration was slightly more massive at 11.64 kg. The chassis was supported along the right edge by bearings sliding on a  $\frac{3}{4}$ " hardened steel rail, and on the left edge by the single wheel to which a rotary encoder was mounted. This configuration allowed for longitudinal translation, but constrained against vertical or transverse motion and rotation in pitch or yaw. Gravity prevented rolling rotation about the rail, ultimately resulting in a one-degree-of-freedom system.



**Figure 15. Close-up view of the motor guide rail.**  
**These linear bushings proved to have too much drag. They were replaced with linear ball bearings.**

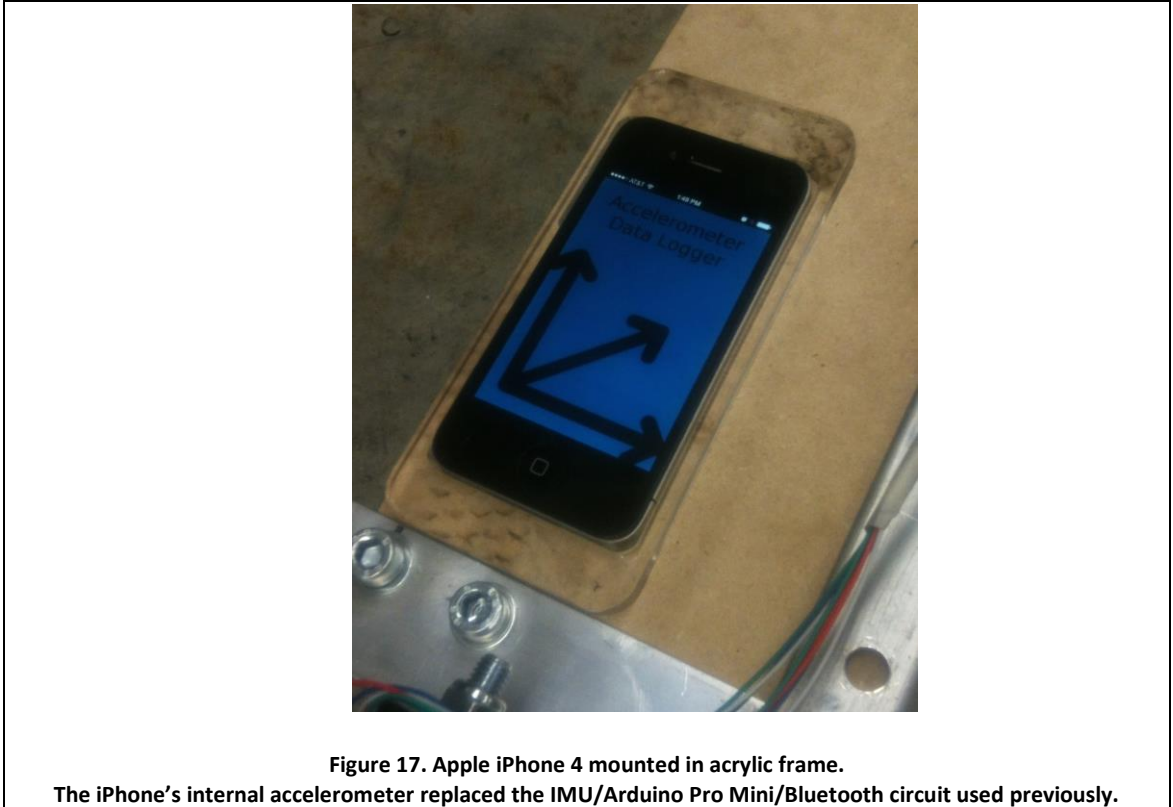
Longitudinal acceleration was originally measured using a Pololu MinIMU-9 v2 inertial measurement unit (IMU). For this application the relevant component of the IMU is a LSM303DLHC 3-axis accelerometer from STMicroelectronics. The acceleration data was collected from the IMU by an Arduino Pro Mini microcontroller and sent to a computer via Bluetooth using a JY-MCU BT\_BOARD module. The accelerometer has a selectable range of  $\pm 2$ ,  $\pm 4$ ,  $\pm 8$ , or  $\pm 16$  g with 12-bit resolution in any range. The  $\pm 2$  g range was selected to give a resolution of 10 bits per g, or just under 0.01 m/s resolution.

After several preliminary datasets had been collected, it was determined that the output of the accelerometer was too noisy to be used in this application. Several filtering methods were attempted, but none were sufficient to reject noise while retaining useful acceleration data. The circuit was abandoned and replaced by an Apple iPhone 4 mounted in a laser-cut acrylic frame secured to the motor chassis. The iPhone contains an LIS331DLH accelerometer (also from STMicroelectronics, offering 16-bit resolution over  $\pm 2$  g, giving accuracy down to about 0.0006 m/s), and a data logging application running at 75 Hz was used to gather data during each run. Log files were then emailed from the iPhone to a computer for analysis.



Also receiving an upgrade after initial trials was the position encoder. Originally a quadrature encoder was constructed using two reflective optical sensors aimed at a strip of alternating white and black bars along the path of travel. The first iteration used a bar pitch of 6 mm. This size was selected so that the (fixed) motor pole pitch of 6 cm would be an even-integer multiple of the (selectable) encoder pitch. However this was found to be too fine a pitch

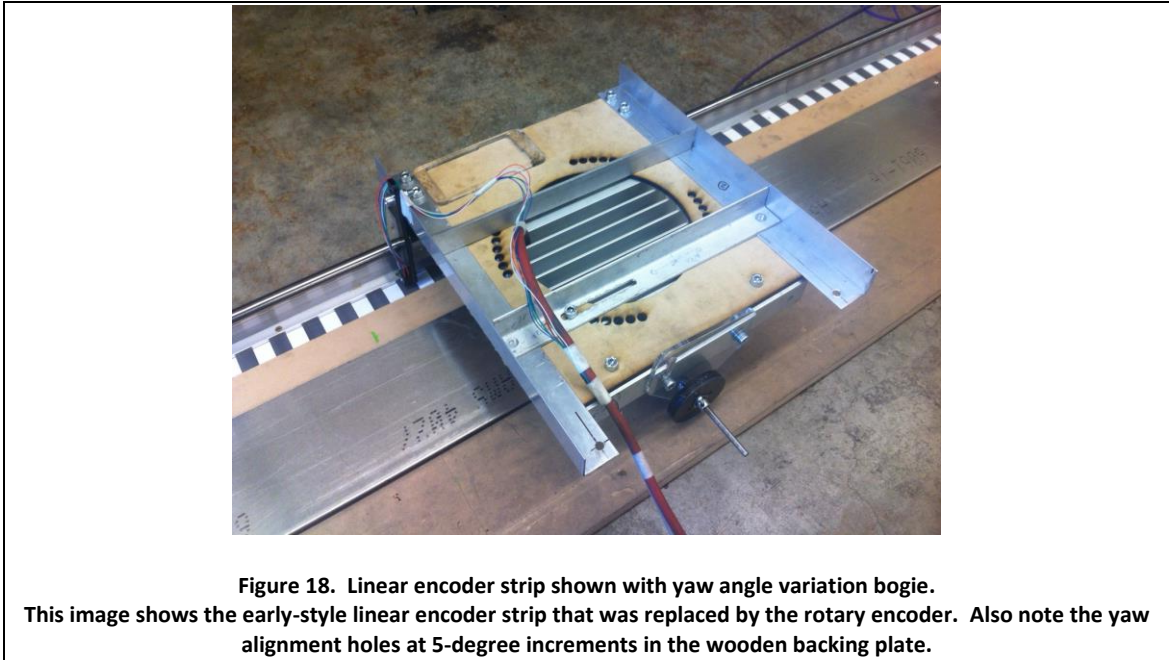
for the sensors to resolve. The pitch was increased until it became reliably resolvable at 2 cm. At this point, the resolution of the encoder was no longer useful, and the design was discarded.



A Heidenhain ERN1080-1024-01 rotary encoder was acquired and attached to the axle of the supporting wheel. The wheel was modified slightly so that one revolution would result in the bogie traveling 12 cm – a distance equal to twice the motor pole pitch. The encoder has a resolution of 1024 counts per rotation, giving 512 counts per pole pitch. The Emerson motor controller requires a power-of-2 resolution per motor pole pitch in order to accurately track position, so this configuration was acceptable.

Static friction was measured using a pull-type force gauge. The force required to overcome static friction was not very consistent. Frequent lubrication of the bearings helped to eliminate some of the variation, but starting force still ranged from 6.2 to 11.1 N. Once the

bogie was in motion, dynamic friction dropped below the instrument's minimum threshold of 5.0 N.



Motor current was measured using inductive loop sensors attached around one of the three motor cables between the VFD and the LIM, and between the VFD and the utility supply.

Baseline data was collected using a 2 mm air gap with the LIM level and aligned with the direction of motion. The VFD was set to a speed ramp from 0 up to 20 HZ. The apparatus was then put through a series of different configurations by adjusting alignment angles about all three axes. Errors introduced consisted of:

- a) Air gap variation in intervals from 2 mm to 9 mm
- b) Pitch angle (about the transverse axis) variation from  $-2^{\circ}$  to  $+2^{\circ}$
- c) Roll angle (about the longitudinal axis) variation from  $0^{\circ}$  to  $+3.25^{\circ}$
- d) Yaw angle (about the vertical axis) variation between the LIM centerline and the direction of motion from  $0^{\circ}$  to  $30^{\circ}$

Once data collection was complete, an alternate bogie and guideway system was implemented. The guideway consisted of a plywood base with parallel wooden side rails. Just as with the previous setup, the steel and aluminum secondary plates were secured along the center of the guideway. The LIM was carried on aluminum brackets supported by four wheels and steered by an additional four wheels rotating in a horizontal plane, rolling along the side rails. A photo of this combination is shown below.



**Figure 19. Alternate bogie and guideway.**  
This configuration aimed to simulate the behavior of a “traditional” bogie-in-guideway design.

Similar data was collected with the LIM attached to this bogie: variation of air gap from 2mm to 9mm, pitch angle from  $-2^\circ$  to  $+2^\circ$ , and roll angle from  $0^\circ$  to  $3^\circ$ . However, the structure prevented any variation in yaw angle, thus that test was omitted.

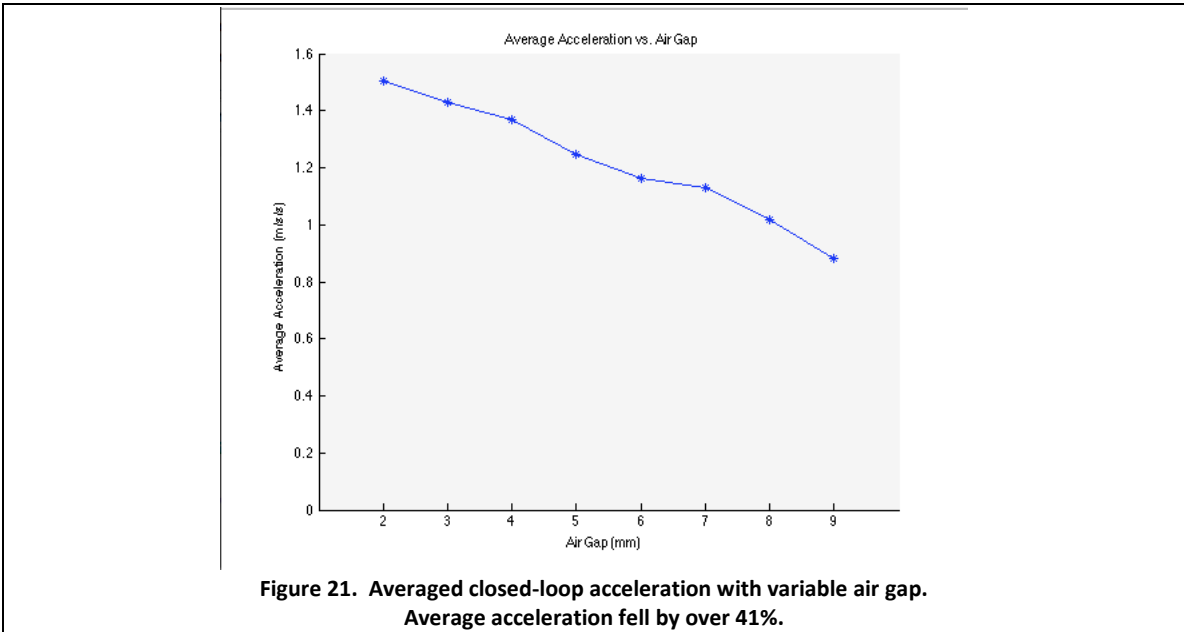
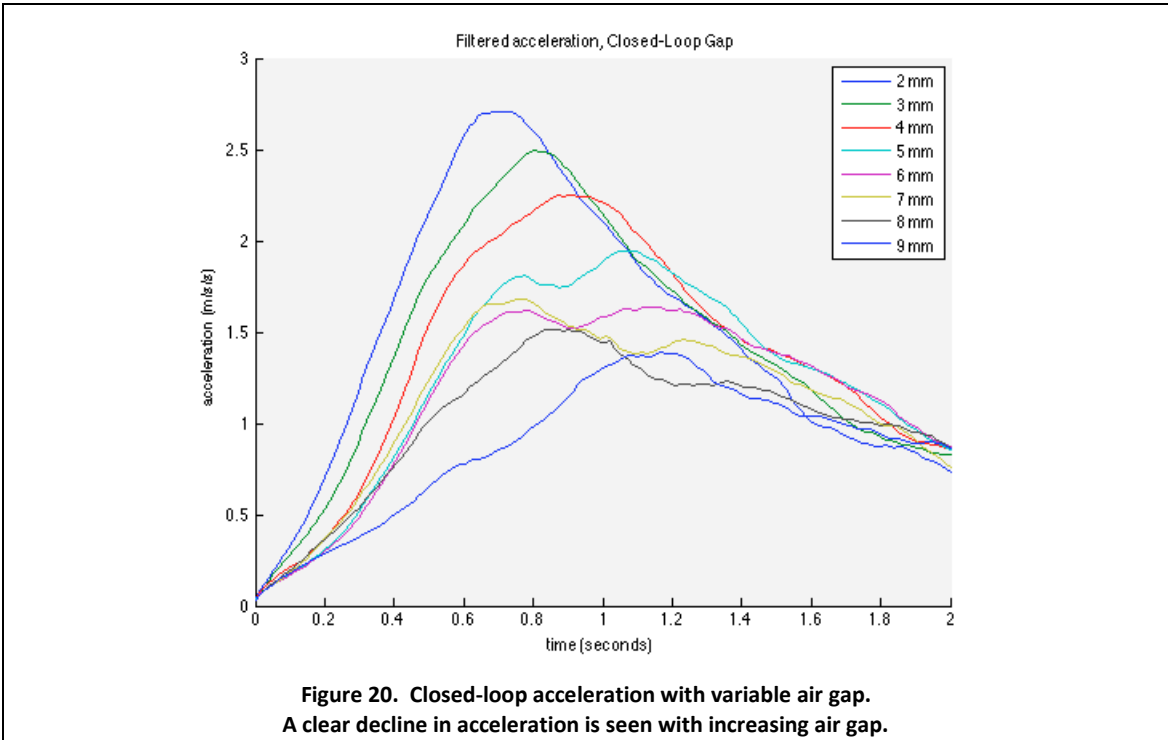
## 3.0 RESULTS AND DISCUSSION

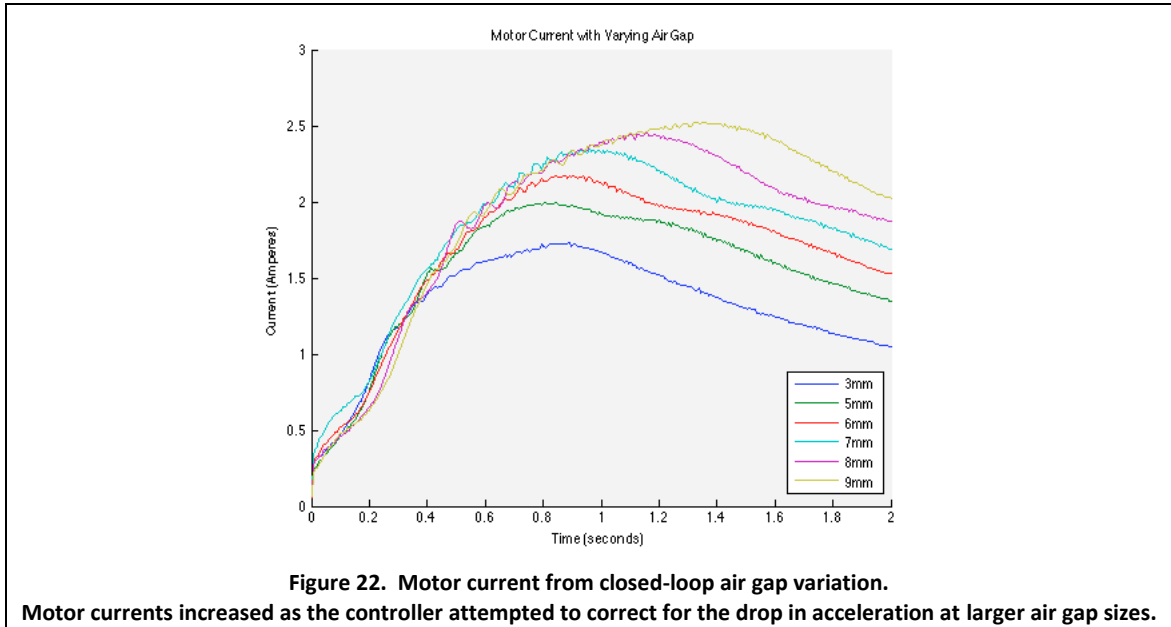
Eighteen repetitions of each run were completed, resulting in a 90% confidence interval that the true mean value lies within one standard deviation of the measured mean for a given configuration. Each line on the following plots represents the average of all of the runs for a given parameter setting. Each of these datasets was then averaged to a single value. For example, every run using a 3 mm air gap was averaged to produce a “typical 3 mm run”, and then every value from the typical run was averaged to produce a single “3-mm value”. This allows a simple, quantitative comparison between configurations.

We discuss each of the parameter variations in sequence. For each parameter, data is presented for acceleration over time, average acceleration, and motor current over time.

### 3.1 Air Gap Variation

Figures 20-22 show the results from varying the air gap between primary and secondary. The manufacturer’s recommended gap is “less than 3 mm”. In this experiment, the air gap ranged from 2 mm to 9 mm in 1-mm increments. Two clear trends can be identified here: as the gap increases, the acceleration drops and the motor current increases.





The average acceleration over the entire run dropped by 41.4% from 1.50 m/s<sup>2</sup> to 0.88 m/s<sup>2</sup>. Motor currents also saw increases as the controller attempted to maintain the commanded acceleration.

In actual operation, a more capable controller should be able to compensate (up to a point) for the increased current demand to continue normal operation in the event of an out-of-adjustment air gap, but the decrease in available thrust is of concern. It is true that the air gap variation tested during this experiment is rather extreme – a threefold increase over the recommended gap – so one might not expect such a dramatic power loss in actual operation. That said, motor-sizing calculations will need to include a sizable safety factor with respect to rated thrust if performance specifications are to be guaranteed even in the case of gross adjustment issues.

### 3.2 Pitch Angle Variation

When discussing pitch (fore/aft tilt) a positive angle indicates the forward edge is above the aft edge, and a negative angle indicates the opposite is true. The LIM was pivoted about its

center, which was kept at a 5 mm air gap. The range of variability in pitch is limited by the length of the motor. Even with the center quite high – almost twice the recommended air gap – the front and rear edges could only vary by 3 mm in height before being in danger of striking the secondary plate. With a larger motor as would be used in a full-scale transit system, it would be nearly impossible to have any significant pitch excursion without an obvious and unreasonable air gap at the raised end of the motor. Nonetheless, to be thorough we explore the LIM's reaction here.

As shown in Figures 23 and 24, a minimal increase in thrust can be seen for a positive versus a negative pitch angle. Given the variation from run to run, this trend may be too small to be statistically significant.

If we make the assumption that it is not simply a random anomaly, this difference may be related to LIM end effects – a phenomenon well known but outside the scope of this project – where the secondary current under the forward portion of the LIM has not had time to fully develop, and is weaker than the current under the aft portion. Even though the average distance from primary to secondary does not change (i.e. the forward edge is raised while the aft edge is lowered) it is more detrimental to thrust production to weaken the more productive portion (the higher-current aft edge) and strengthen the less productive portion (the lower-current forward edge) than vice-versa.

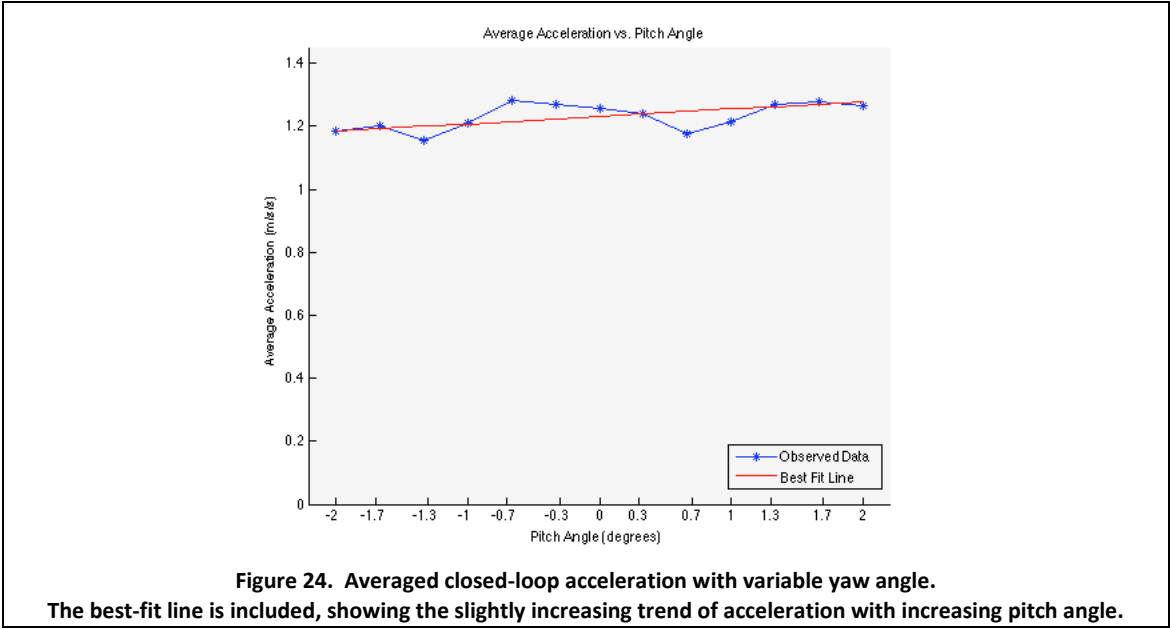
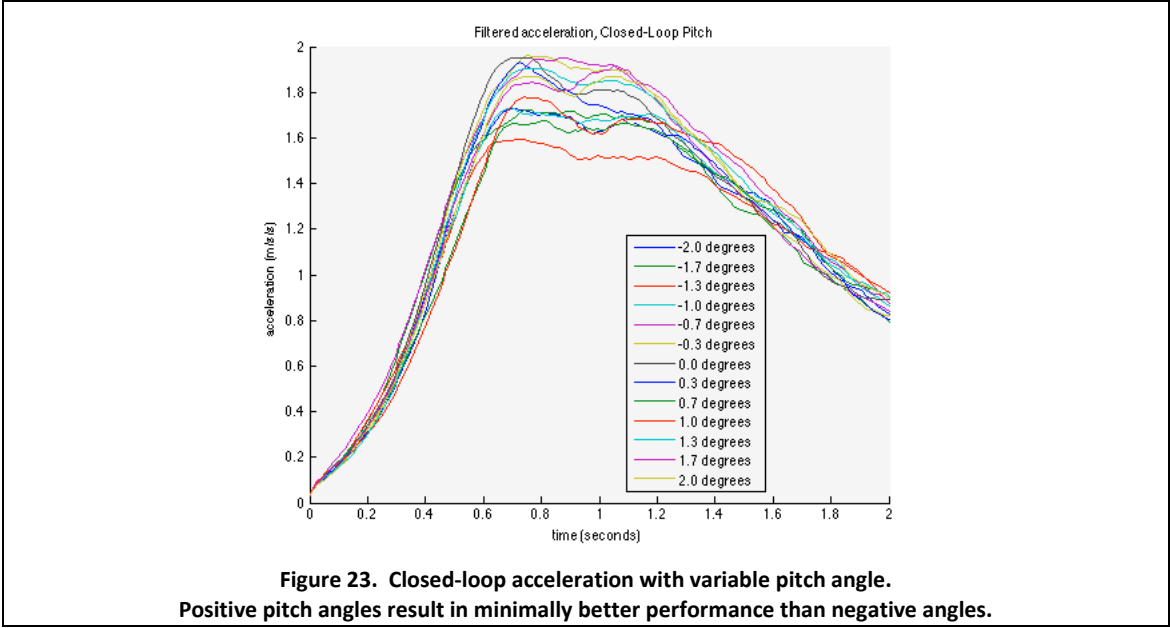
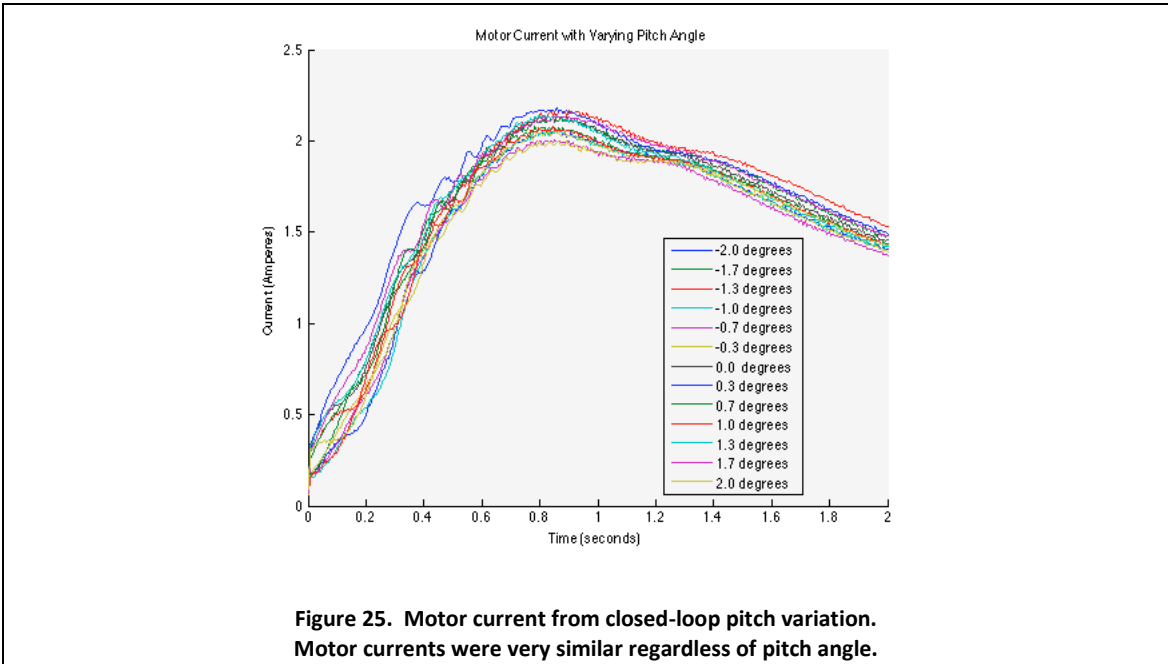
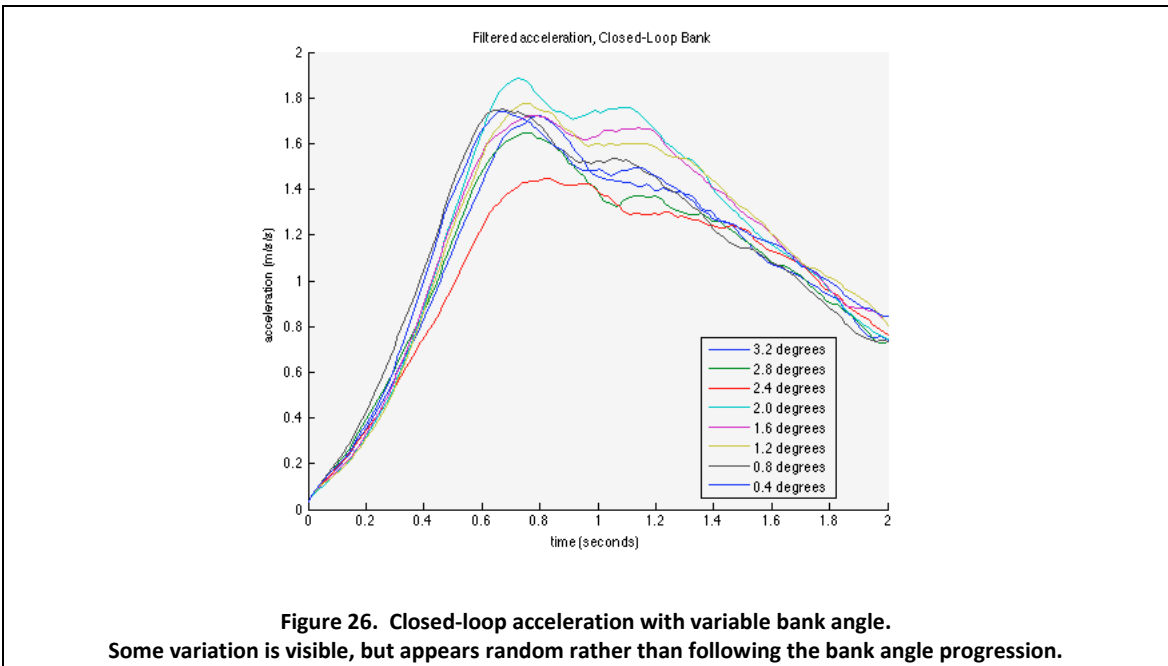
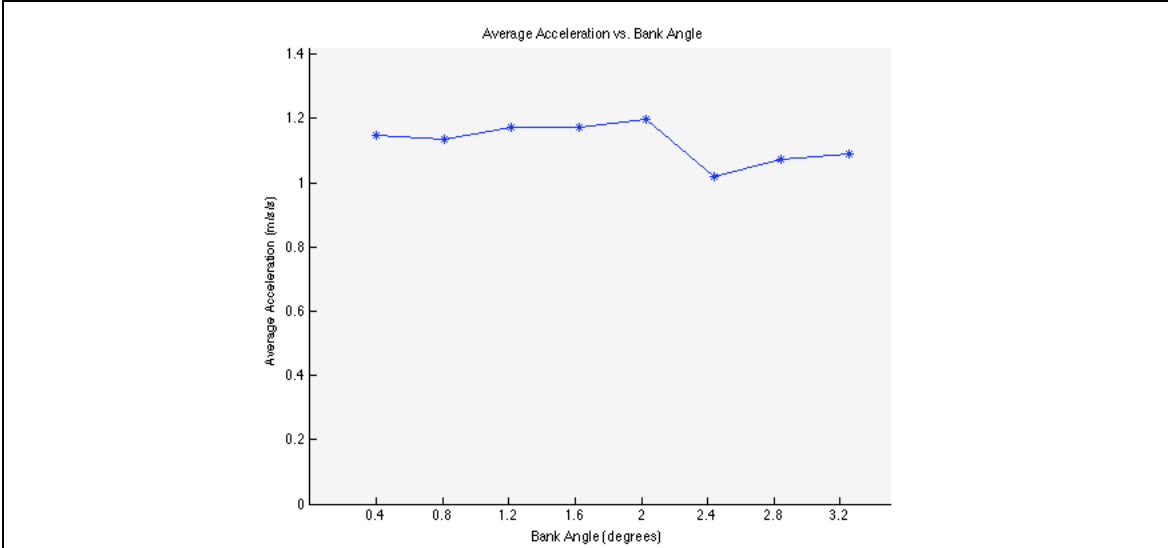


Figure 25 below shows the motor current for varying pitch angles. No clear trend was identified with regard to increased or decreased pitch.



### 3.3 Bank Angle Variation





**Figure 27. Averaged closed-loop acceleration with variable bank angle.**  
 As noted previously, changes in acceleration do not appear to correlate with bank angle.

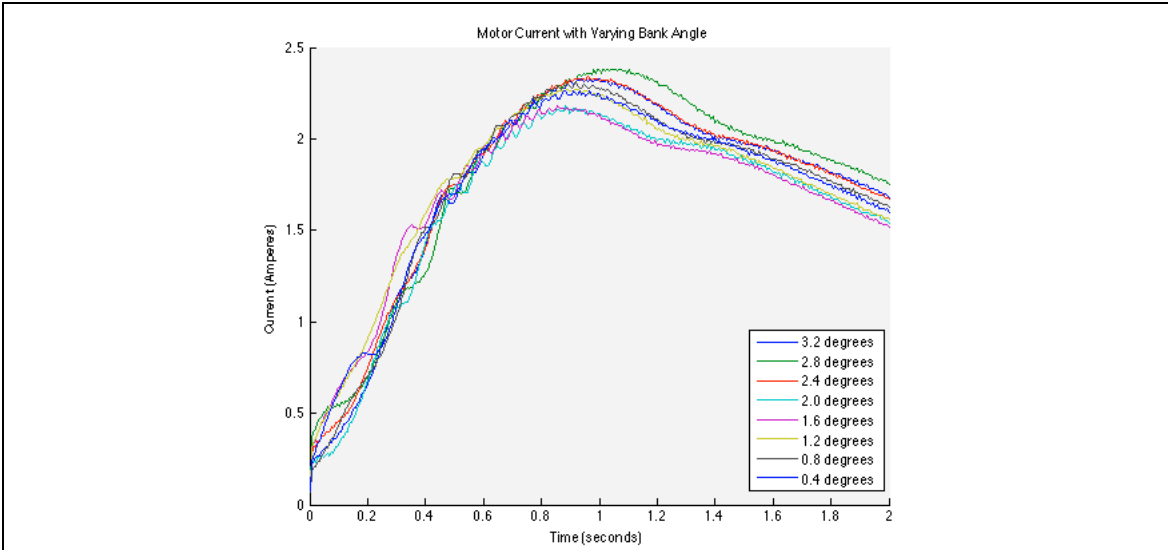


**Figure 28. Motor current from closed-loop bank variation.**  
 Though different configurations are clearly striated, their relative levels do not vary predictably with bank angle.

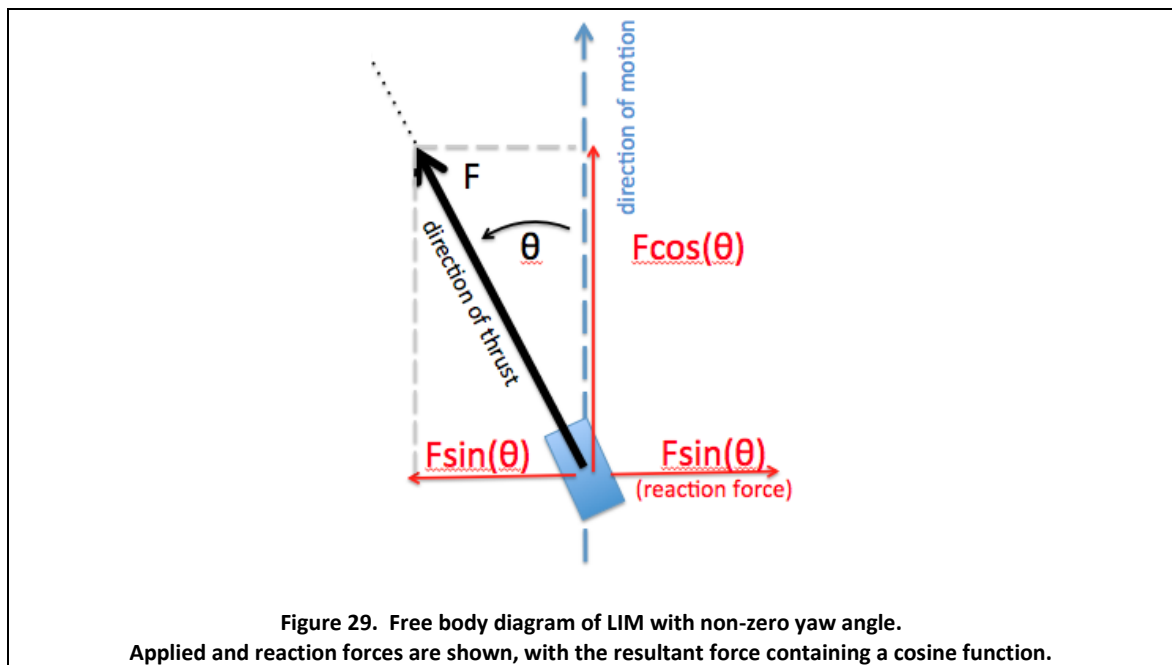
Each phase winding runs the width of the motor from side to side, so the overall average distance between any given coil and the secondary did not change. Essentially, we expect to see losses in the raised portion of the motor that are balanced by performance improvements in the lowered portion.

Moving along the progression of bank angle, we find relatively flat acceleration except for the abrupt drop between 2.0 and 2.4 degrees. Above and below this level, adjacent data points are similar, possibly indicating a defect introduced in the experimental setup between those sets.

Similarly to pitch, the bank angle excursion is limited by the size of the motor. A large gap will result along the left or right edge before a significant bank angle can develop, thus in practice the effect of a non-zero bank is largely moot.

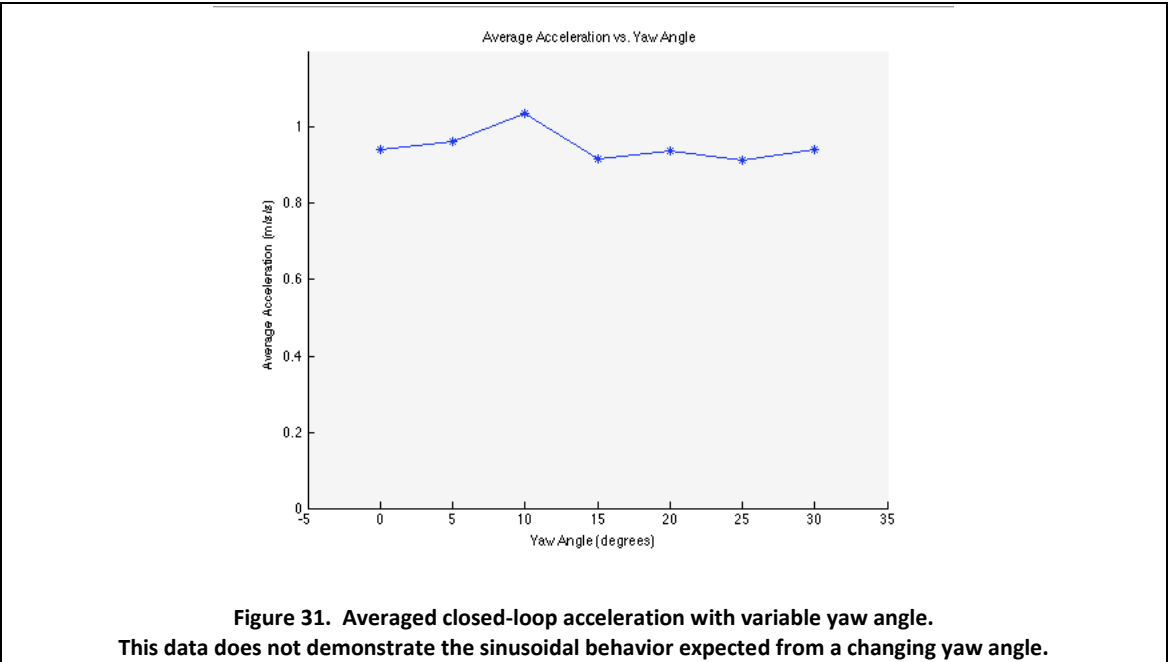
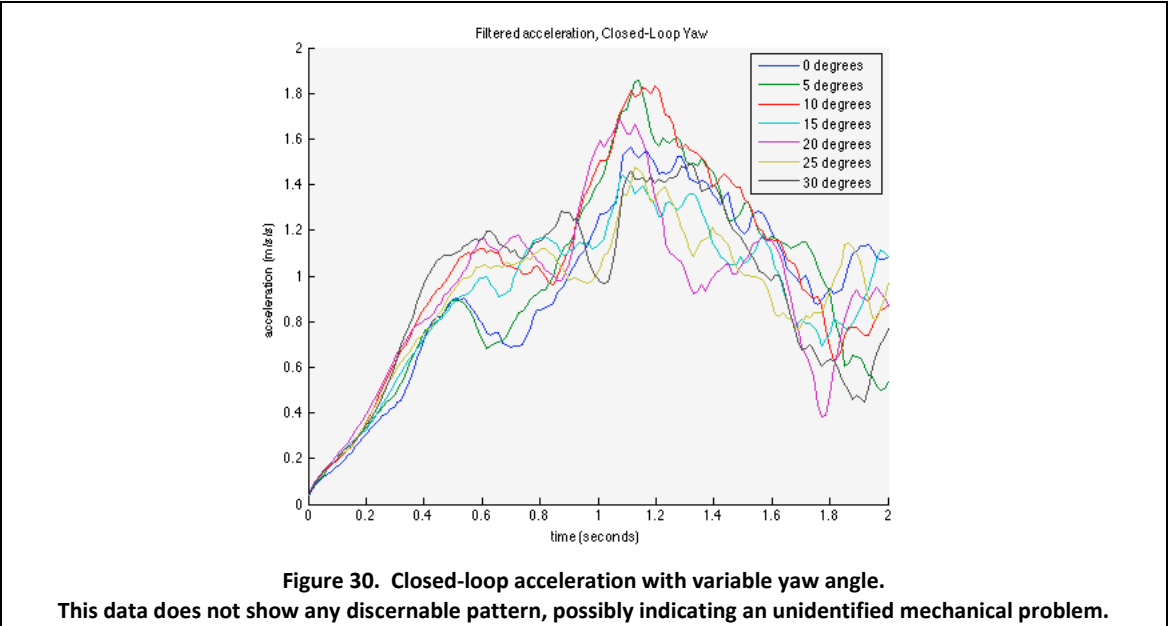
### 3.4 Yaw Angle Variation

If we consider a free body diagram representing the LIM with variation in its yaw angle, we expect to see a decrease in forward thrust that scales with the cosine of the yaw angle.

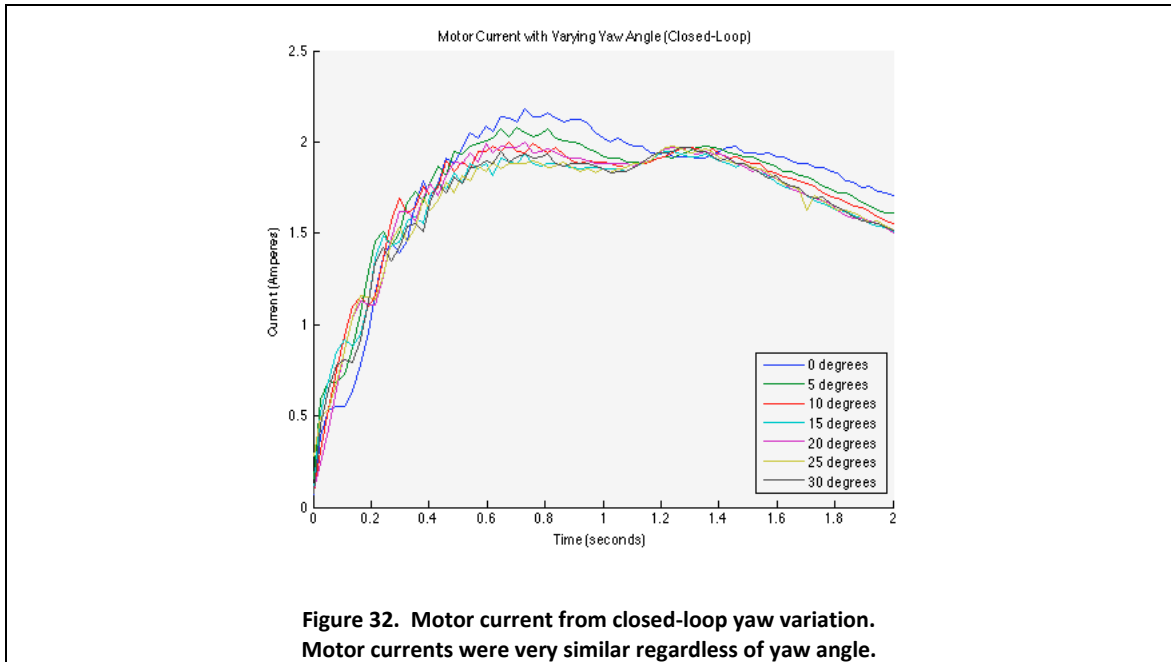


Only the component of thrust aligned with the direction of travel can perform useful work. Thus, even ignoring other effects of the LIM, we expect a decrease in acceleration with increasing yaw angle.

As may be seen in Figures 30 and 31, no discernable pattern is apparent. Unlike the other parameter variations, no progressive change – sinusoidal or otherwise – occurs with an increase in the yaw angle, and differences in acceleration between different configurations appear random. The plot of average accelerations is generally flat, rather than sinusoidal as expected.



Initially one might believe that the motor controller is simply doing an excellent job compensating for the reduced forward thrust vector, but examining the motor current plot in Figure 32, a corresponding increase in current is not found. In fact, motor current levels are largely indistinguishable except at the lowest yaw angles, where they are slightly higher.



For the gap, pitch, and bank studies, the LIM was always aligned with the direction of travel, allowing the supporting structure (linear bearings and wheel/encoder) to be attached directly to the side of the LIM. A separate mounting plate was used for the yaw dataset in order to allow the LIM to be aligned away from its direction of travel.

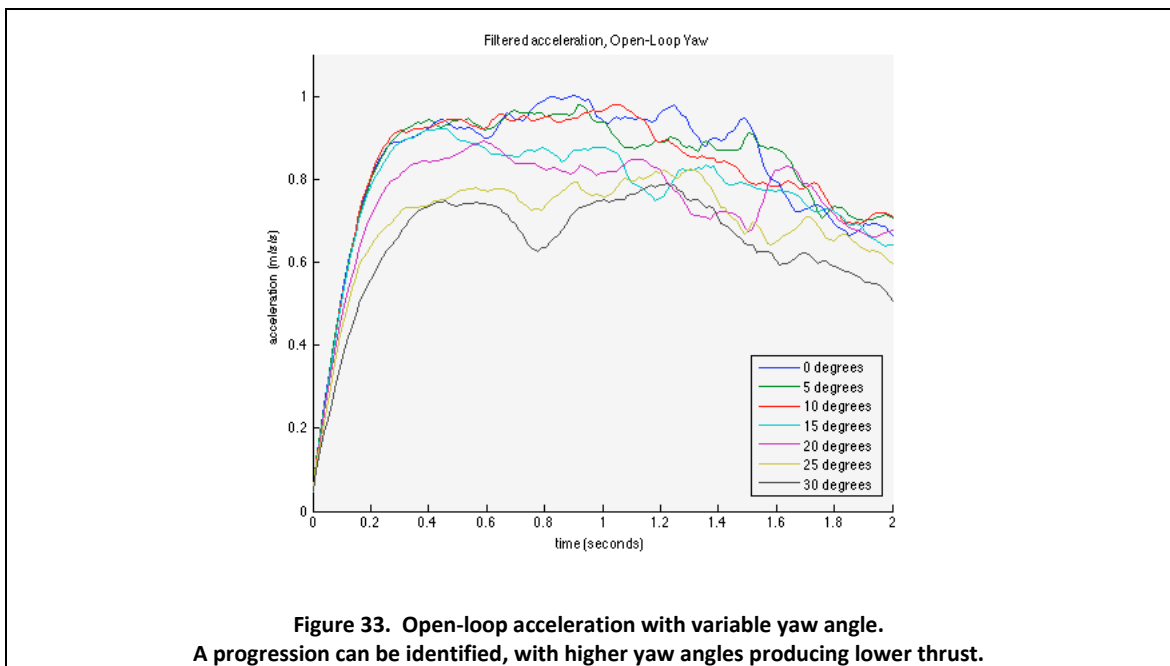
Open-loop trials with variation of air gap, pitch angle, and bank angle were completed first as a set, then the bogie was changed to the yaw angle variation setup. Once this was finished, the bogie was switched back to the original configuration for closed-loop tests, then back to the yaw setup once again to complete the set. It is believed that something was amiss during this final closed-loop yaw test, and this led to the random nature of the data. As the lab facility and LIM equipment are no longer available, the discovery and remedy of this defect is left to future work.

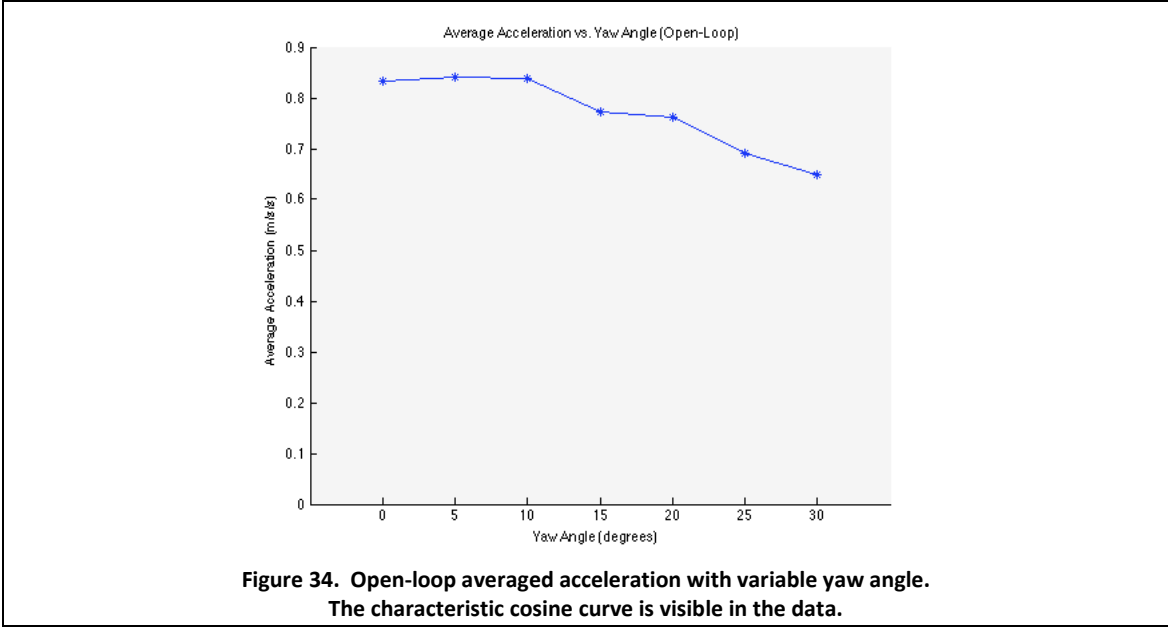
Instead, we look to the data collected using the earlier open-loop control algorithm. Many control parameters were changed when switching from open loop to closed loop control, so the reader is cautioned against direct comparison to other datasets. However, there is still some benefit to be gained from considering this data.

Most obviously in Figure 34, we begin to see approximately the cosinusoidal decrease originally expected.

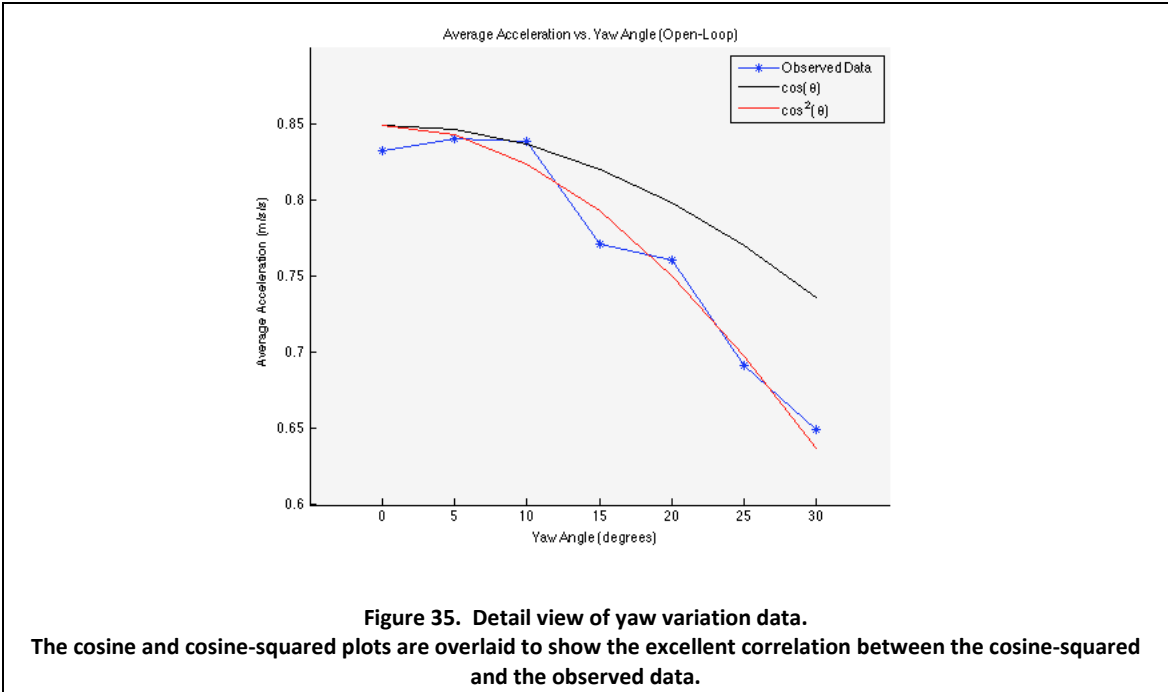
Upon closer inspection while expanding the vertical axis (see Figure 35), it is noted that the measured acceleration decreases with increasing yaw angle slightly more sharply than the cosine of the yaw angle. In fact, with the square of the cosine overlaid on the data, we see that there is a good correlation between the two.

This also follows logically given the geometry of the LIM setup. The component of thrust normal to the direction of travel is absorbed by the mechanical constraints of the system. But even before that, there is a loss of thrust produced by the LIM. As the flux vector travels along the length of successive LIM coils, it induces currents in the area of the secondary plate





beneath it. Under normal conditions, the LIM is constantly moving over a new area, and the induced currents will appear to propagate along its length. (The opposite is actually true- it is the LIM that propagates over the stationary plate.)



With the LIM misaligned, successive coils along the length of the LIM will pass over new areas of the secondary plate that have not been fully exposed to the primary flux due to the

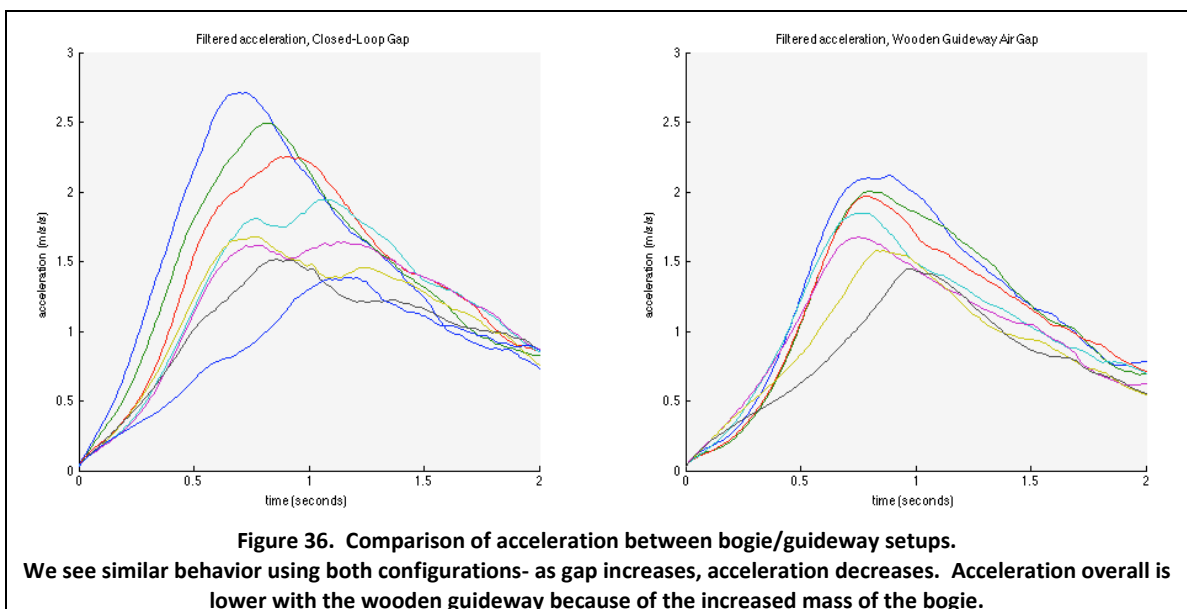
skidding nature of the LIM motion, and thus have lower induced current. The amount of this reduction is geometrically determined by the yaw angle, and is itself a cosine function. The total thrust will be the product of these two independent cosine functions, and we then observe the cosine-squared result.

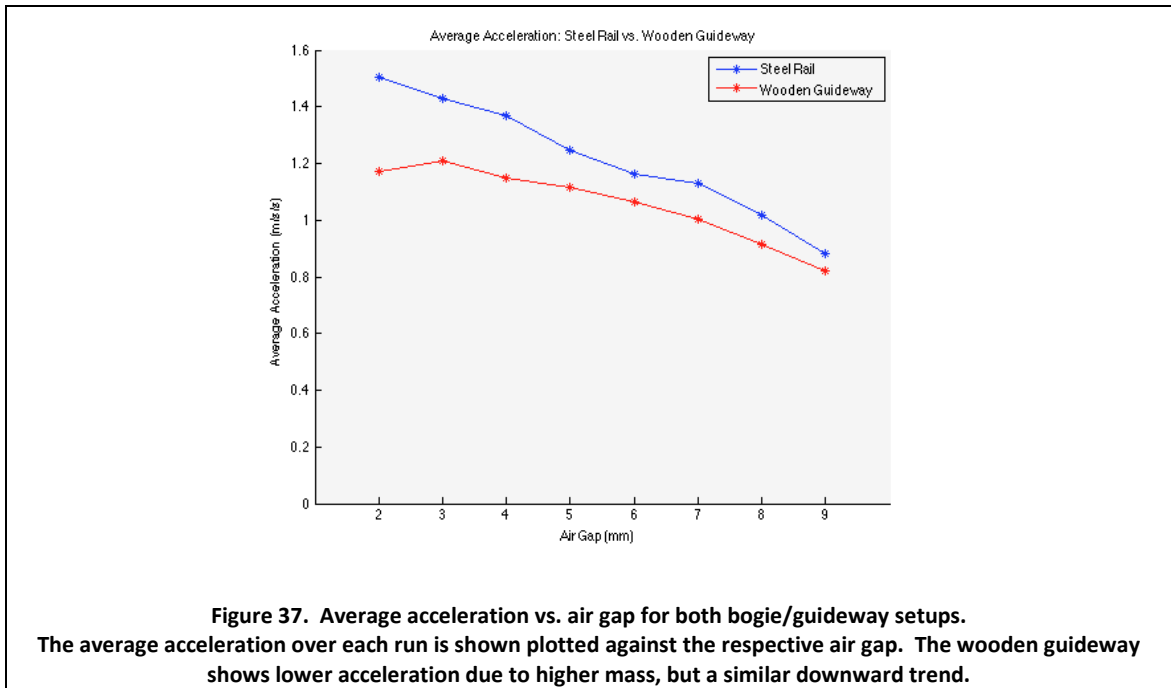
### 3.5 Testing Using Wooden Guideway

Once all of the closed-loop data was collected, the LIM and secondary plates were transferred to the alternate bogie and guideway. This bogie was somewhat more massive at about 14.8 kg, thus even for the same thrust output we expect correspondingly lower acceleration values.

#### 3.5.1 Air Gap Variation

Figure 36 shows the closed-loop air gap data (left) beside the air gap data from the wooden guideway/bogie (right) for comparison. As expected, we see lower overall acceleration with a downward trend as the size of the air gap increases. Other than this mass-proportional decrease, no significant differences from the original bogie design were discovered.





### 3.5.2 Bank Angle Variation

Unlike the previous dataset, we do not see an overall decrease in acceleration in the wooden guideway versus the steel rail setup for the bank angle variation study. Little to no correlation was expected between bank angle and acceleration, but the more massive bogie should have caused lower acceleration in all configurations. As can be seen in Figure 38, peak acceleration on the wooden guideway is actually slightly higher than the original dataset. The cause remains unexplained.

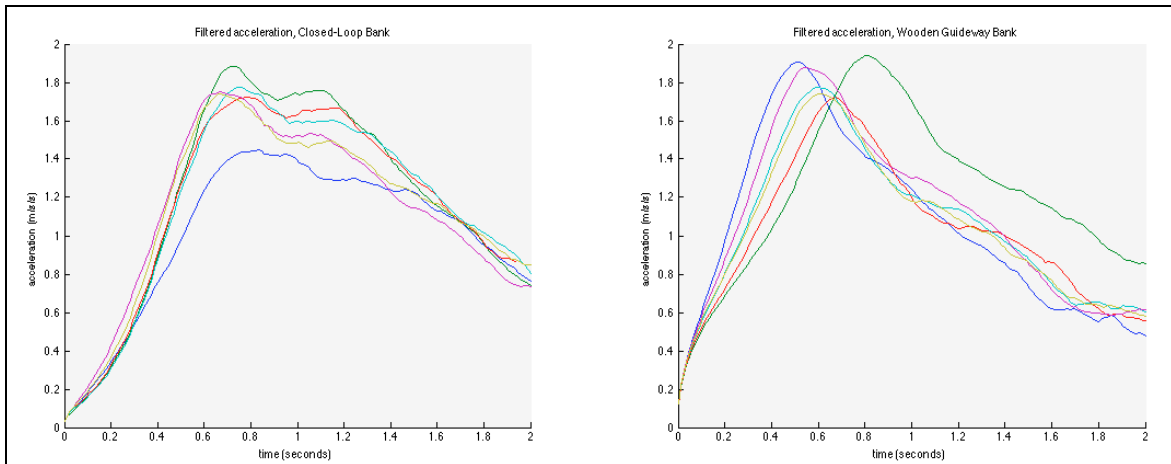


**Figure 38. Acceleration vs. bank angle for both bogie/guideway setups.**  
 Each line represents the average run for a given bank angle. As predicted by the steel rail data, no discernable pattern is found by varying the bank angle. Note that the expected lower overall acceleration due to the more massive bogie is not observed.

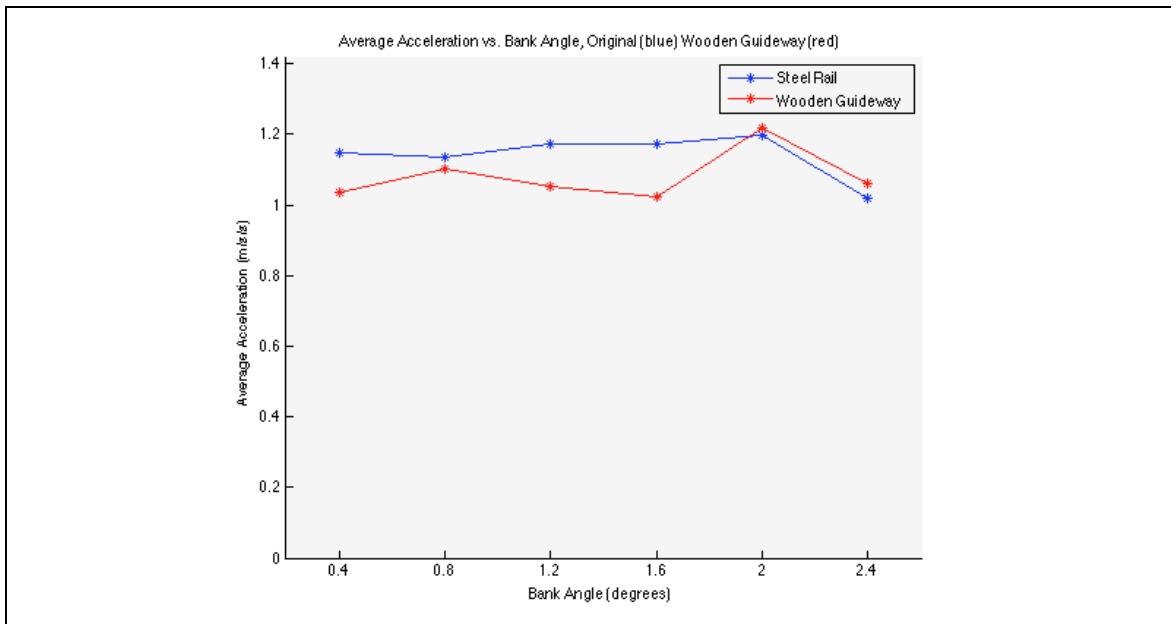
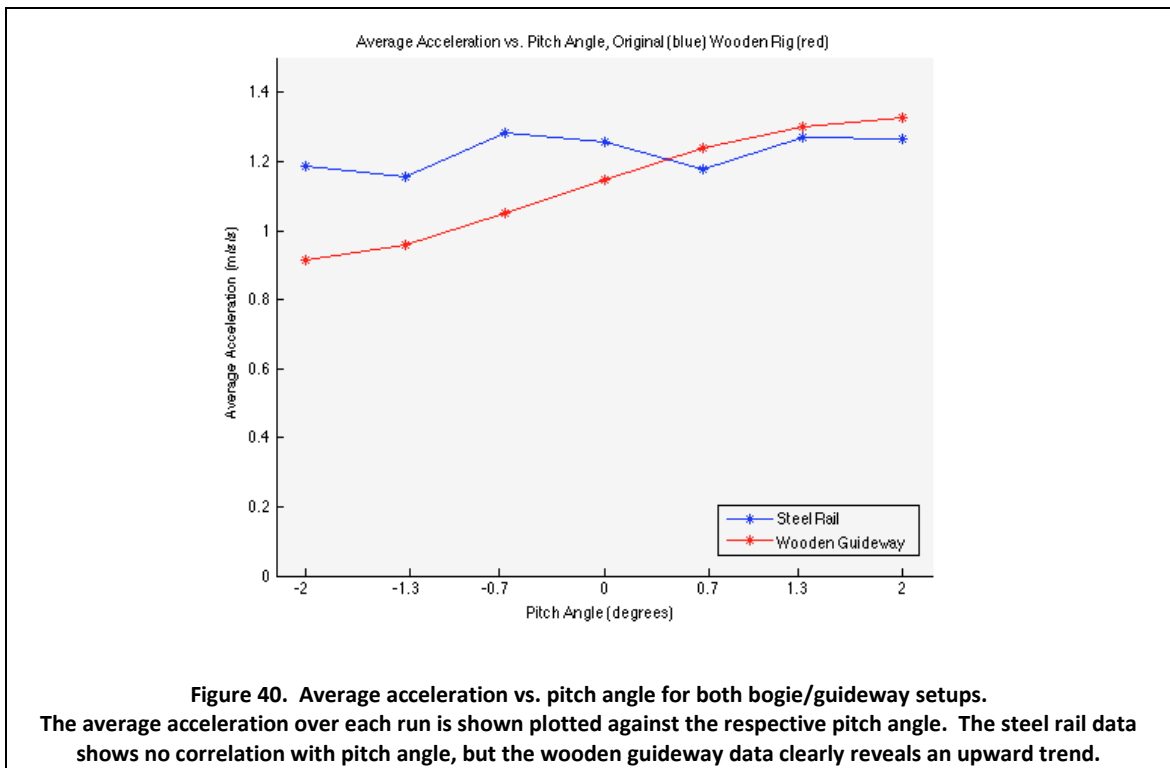


**Figure 39. Average acceleration vs. bank angle for both bogie/guideway setups.**  
 The average acceleration over each run is shown plotted against the respective bank angle. No discernible trend is identified with varying bank angle.

### 3.5.3 Pitch Angle Variation

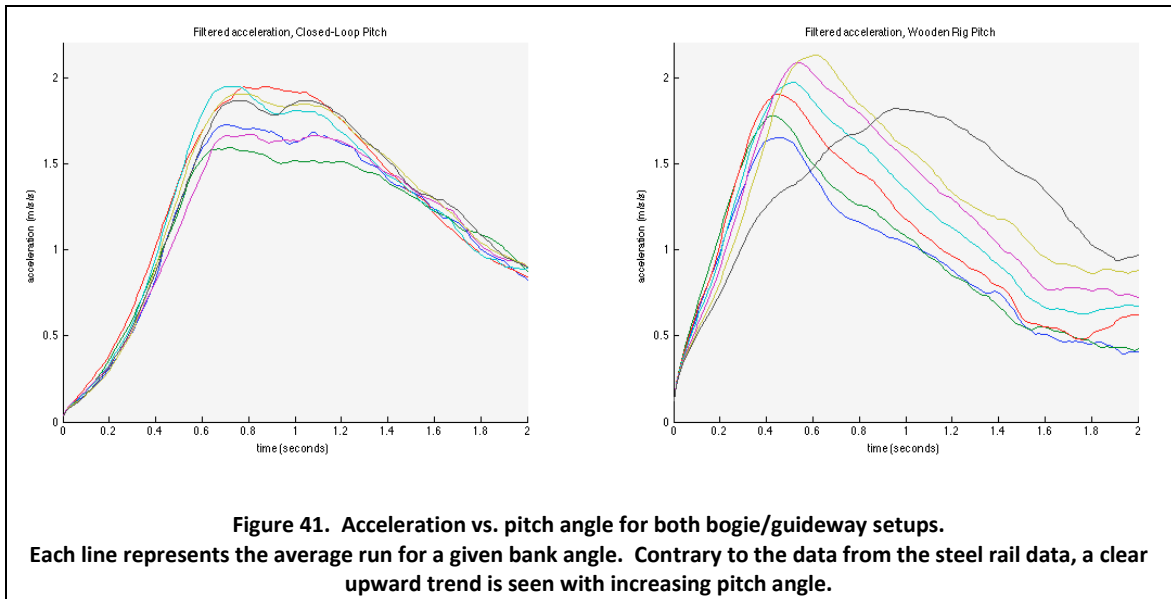
Once again we find unexpected behavior in the final dataset. As described earlier in section 3.2, varying the pitch angle did not have a significant effect on acceleration. Given equivalent thrust output using the more massive bogie on the wooden guideway we expect to see a decrease in acceleration proportional to the increased mass. However, neither of these cases was borne out in the final trial.

With regards to the pitch angle, no significant correlation was found in the steel rail dataset, but a consistent increase in acceleration is obvious with increasing pitch angle on the second apparatus (see Figure 40 below). A two-degree positive pitch results in a 45% increase in thrust over a two-degree negative pitch.



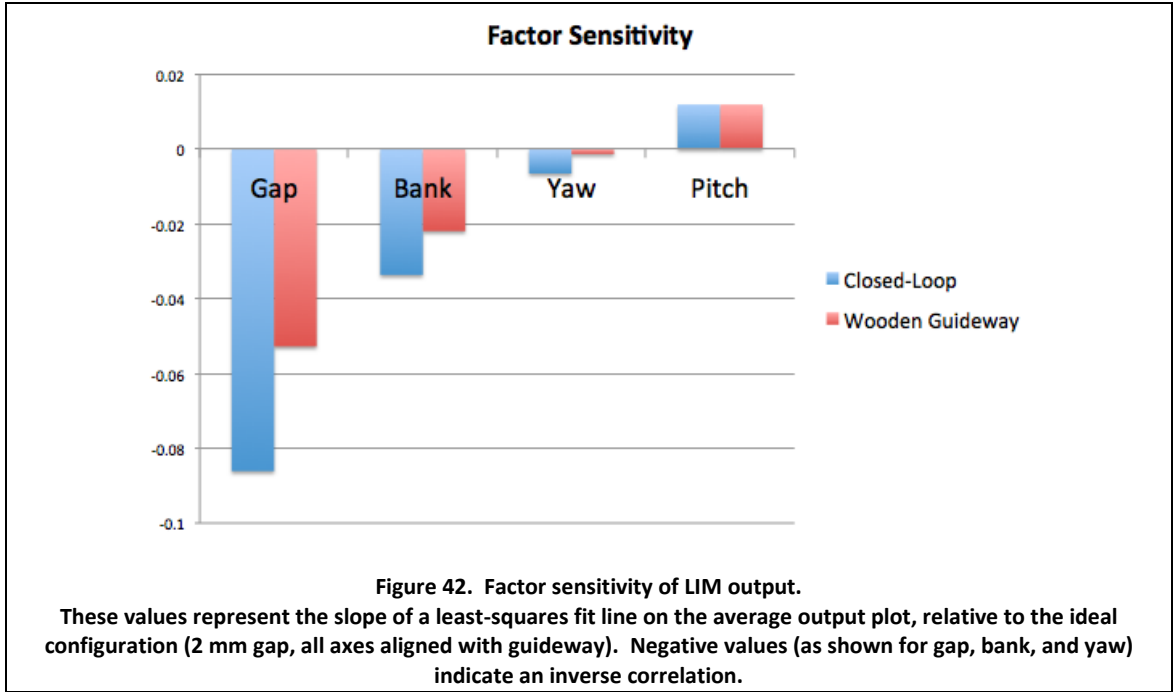
In addition, the increase in bogie mass did not produce the expected decrease in acceleration. Peak acceleration values on the wooden guideway are again observed to be

slightly above the values recorded using the steel rail guideway, rather than the  $\approx 40\%$  reduction expected.



### 3.6 Factor Sensitivity

It is clear that variation of each parameter- air gap, pitch, bank, and yaw- affects the motor output to varying degrees. Here we summarize the relative influence of each factor on each of the bogie/guideway combinations. This is accomplished by finding a best-fit line to the plot of each parameter's output. The slope of this line will indicate the impact that each factor has on the overall thrust. The results of this analysis are shown in Figure 42 below.



Note that, as expected, the factors are ranked identically for either configuration. The difference in sensitivity between configurations aligns well with the relative mass of the bogies. Figure 42 shows about 63% difference between the two. Given the bogie masses of 10.17 kg and 14.8 kg, they differ by 68%.

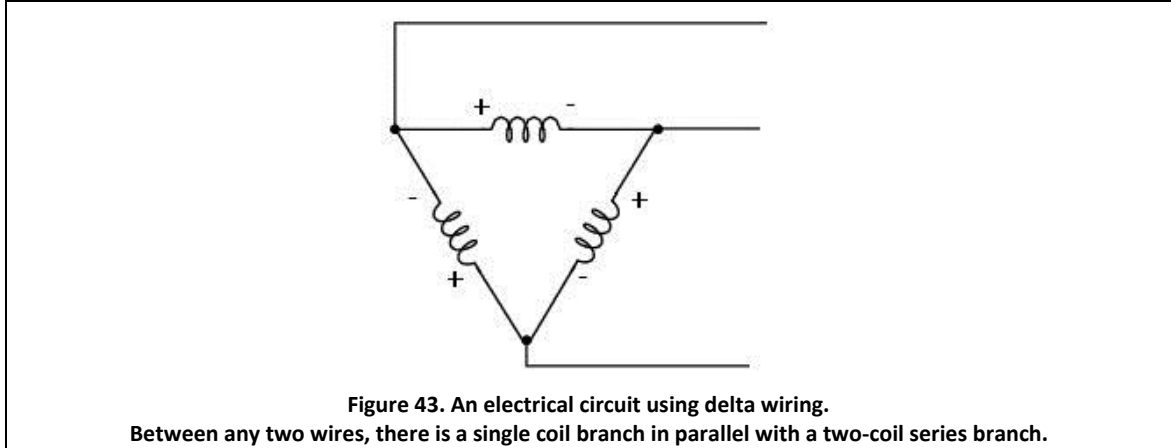
### 3.7 Electrical Power and Efficiency

Electrical power is easily calculated using motor phase current and resistance:

$$P = I^2 R \tag{8}$$

We examine the data from the air gap variation runs. Motor phase current was measured for several runs of each setting. The resistance between motor poles was measured as 40 Ω. Recall that this motor is wired in a delta configuration, thus the single-phase resistance is calculated to be 60 Ω as shown in Equation 9.

$$\frac{1}{R_{measured}} = \frac{1}{R_{phase}} + \frac{1}{2R_{phase}} \rightarrow R_{phase} = \frac{3}{2} R_{measured} \tag{9}$$



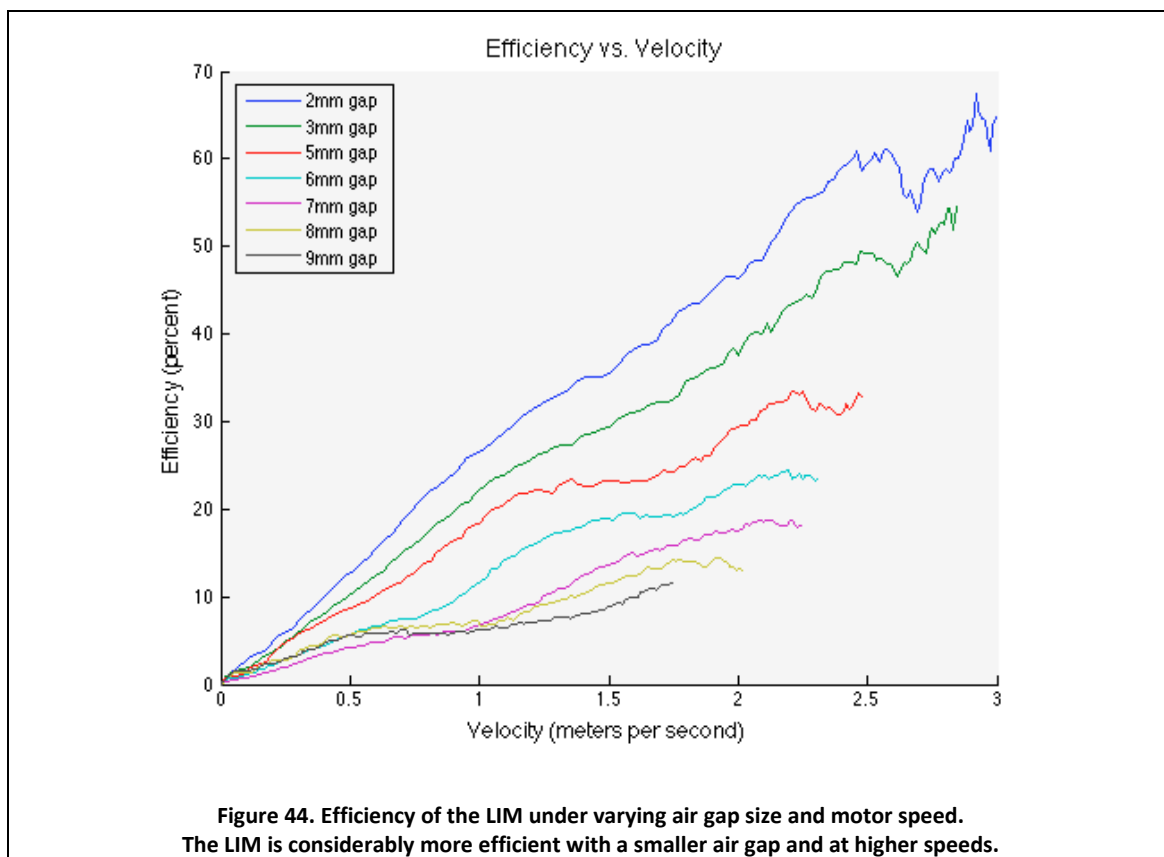
Since instantaneous current and resistance are known, instantaneous power is easily calculated. Electrical efficiency may be determined by comparing the electrical power applied to the motor to the mechanical work performed. Work is defined as a force applied over a distance, while mechanical power is work per unit time. Newton’s second law gives us the equation to determine the force applied to the bogie:

$$Force = mass \times acceleration \tag{10}$$

The instantaneous acceleration was measured and the mass is constant, so the force being output by the motor may be calculated. Thus, efficiency is calculated using equation 11:

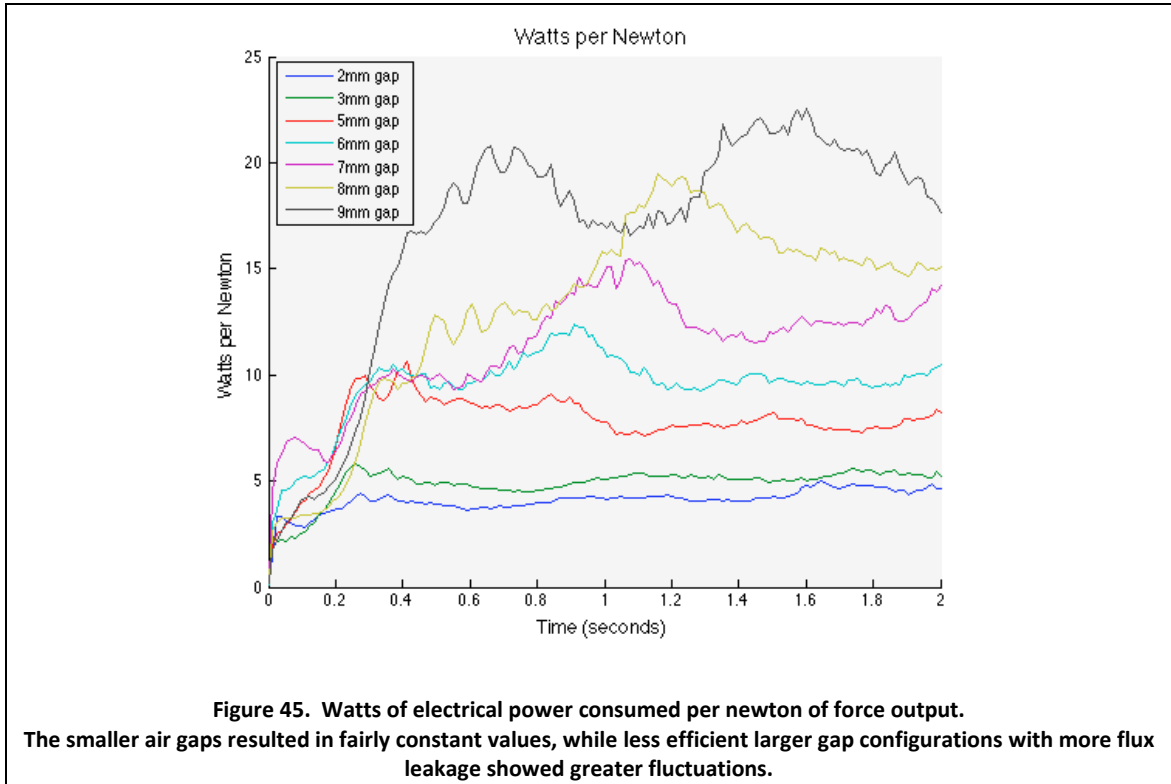
$$Efficiency = \frac{mechanical\ power}{electrical\ power} = \frac{\left(\frac{mass \times acceleration \times distance}{time}\right)}{current^2 \times resistance} \tag{11}$$

Unsurprisingly, LIM efficiency is greatest with a small air gap. As seen in Figure 30 below, with a 2 mm air gap the motor efficiency approached 70% at the end of the test interval. Larger gaps performed more poorly, with a 9 mm air gap barely reaching 10% efficiency.



For comparison, US Department of Energy regulations set minimum efficiency standards for motors that are in use for more than 500 hours per year. These minimums vary based on motor rating and number of poles, but motors above about 7.5 kW require efficiencies above 90%, with more stringent requirements as power increases (NEMA, 2008).

We can also calculate the output of the motor in terms of watts per newton (W/N). The electrical power has already been calculated; now we divide by the instantaneous force to find the data shown in Figure 45. For smaller values of air gap, the efficiency curve is quite flat at around 4 to 5 W/N. However as the air gap grows, leakage flux increases leading to lost energy and thus lowering the efficiency. This poorer efficiency makes thrust more costly as the input power required for a given output force increases considerably.



### 3.8 Motor Sizing Considerations

The Force Engineering F951 LIM used to collect the above-described data is a small unit not designed for use in transit vehicles; a larger, more powerful motor will be required for the full-size system. As discussed earlier in section 1.2.2, maximum acceleration limits for a service vehicle are determined by human factors.

A short-primary system with the motor mounted to the vehicle will require a high duty cycle, because all thrust must be produced by a small number of LIMs (usually 1 to 4 units mounted to the bogie), where a LIM in a long-primary system is only active while the vehicle is passing a given point on the guideway, requiring a much lower (usually <10%) duty cycle.

The maximum allowable duty cycle will decrease as the thrust output of a LIM increases due to power dissipation and equipment cooling requirements. Employing aggressive heat transfer methods and devices can increase the allowable duty cycle, but this will add mass and

bulk to the bogie or guideway, as appropriate. Most manufacturers limit LIM duty cycles at maximum thrust output to levels below 5% for units without active cooling.

What this ultimately means is that producing the ~2 kN of thrust at near 100% duty cycle needed for normal acceleration would necessitate a massive combination of LIM and cooling equipment. Given Superway's goal of a visually compact guideway and bogie, such a motor will likely be much too large, thus precluding the short-primary model.

LIMs are commercially available (such as H2W Technology's LMG-06-650-SSE [H2W, 2011]) that can meet or exceed Superway's thrust needs at a 2-3% duty cycle using the higher voltage range (~400 V) common in high-power transit applications. This H2W unit could be mounted inside the guideway with a minimum motor pitch of approximately one meter, ensuring consistent linear coverage.

## **4.0 CONCLUSIONS AND RECOMMENDATIONS FOR FUTURE WORK**

This project has succeeded in setting up a LIM on a small track and testing output under suboptimal conditions. In the case of pitch or roll angle, significant deviations are nearly impossible to encounter, as they are limited by the large size of the LIM relative to a very small gap. Yaw angle deviations are possible, but become obvious to even a casual observer before becoming large enough to contribute significant degradation to the system. The most likely fault condition is a larger-than-normal air gap. It has been shown that a LIM operating in such conditions produces a degraded but predictable response, and given adequate compensation in the design of the system, LIMs can be a viable option for Superway.

A short-primary model will likely be too bulky and result in a bogie that is too large to be accommodated by a reasonably sized guideway. However a long-primary system could be implemented with existing technology that meets the design requirements for an ATN, provided

the air gap can be kept very small. Electrical efficiency falls off very rapidly with even a small increase in air gap, so this design point should be given every consideration.

The main advantages of LIMs over rotary motors are the independence of thrust from surface traction, and the reduction of moving parts. The decision must be made regarding the value of these features compared to the lower efficiency (higher operating costs) and critical design dimensions (higher manufacturing costs).

Regarding future work, it may be advantageous to construct a bogie that travels on a circuit rather than simply in a straight line. This would allow testing at higher speeds and for longer duration, as the length of the track would not limit each test run. Data could be collected at steady state, rather than only during initial acceleration. Alternative control algorithms could be explored. It may also prove useful to build a similar bogie powered by a rotary motor to offer more direct comparison of performance.

Likely the greatest improvement to LIM technology would be active control of the air gap size. If the LIM height and thus air gap were dynamically adjustable rather than needing to accommodate the worst case tolerance stack up for each component, significant performance and efficiency gains could be realized. Such a modular LIM carriage and air gap control system would be very helpful.

## REFERENCES

2getthere. "Masdar PRT Application." Internet: [http://www.2getthere.eu/?page\\_id=10](http://www.2getthere.eu/?page_id=10), 2012, [Oct. 13, 2013].

A. Ampère. *Mémoire sur la théorie mathématique des phénomènes électrodynamiques uniquement déduite de l'expérience (Memoir on the Mathematical Theory of Electrodynamical Phenomena, Uniquely Deduced from Experience)*. Paris: Mequignon-Marvis, 1827.

A. Binder, M. Hofmann, and R. Pfeiffer. "Investigations on a linear induction machine for railway applications," in Proc. IEMDC-IEEE, 2001, pp. 20-26. DOI: 10.1109/IEMDC.2001.939267

B. Burlingame, A. Davis, et al. "Superway: A Solar Powered Automated Transportation System." San José State University, May 13, 2013.

Cabintaxi. "Cabintaxi PRT System." Internet: <http://faculty.washington.edu/jbs/itrans/cabin.htm>, Sept. 20, 2012. [Mar. 28, 2014].

California Energy Commission Consumer Energy Center. "Energy Losses in a Vehicle." Internet: [http://www.consumerenergycenter.org/transportation/consumer\\_tips/vehicle\\_energy\\_losses.html](http://www.consumerenergycenter.org/transportation/consumer_tips/vehicle_energy_losses.html), [Nov. 16, 2013].

The Daily Courier. "Winter storm spreads rain, heavy snow across state." Internet: <http://www.dcourier.com/main.asp?SectionID=1&SubSectionID=1086&ArticleID=116868>, [Dec. 9, 2013].

S.S. Fazel and S. Motlagh. "Indirect Vector Control of Linear Induction Motor Considering End Effect." Power Electronics and Drive Systems Technology (PEDSTC), 2012 3<sup>rd</sup>, pp. 193-198. DOI: 10.1109/PEDSTC.2012.6183324

Force Engineering. "Linear Induction Motor Options." Internet: <http://www.force.co.uk/linear-motors/lim-options.php>, [Sep. 6, 2013].

A. Gastli. "Electromechanical systems and actuators, linear motors." Internet: [http://emsa.gastli.net/Chapter8/Linear\\_Motors.pdf](http://emsa.gastli.net/Chapter8/Linear_Motors.pdf), [Sep. 6, 2013].

H2W. "AC Linear Induction Motor." Internet: <http://www.h2wtech.com/Products/ShowProduct?productid=231>, [Aug. 21, 2014].

Hellinger, R.; Mnich, P., "Linear Motor-Powered Transportation: History, Present Status, and Future Outlook," *Proceedings of the IEEE*, vol.97, no.11, pp.1892,1900, Nov. 2009.

Hoberock, L. L. "A Survey of Longitudinal Acceleration Comfort Studies in Ground Transportation Vehicles." *Journal of Dynamic Systems, Measurement, and Control* 99, 1977, pp 76.

P. Hsu. EE 237. Class Lecture, Topic: "Permanent Magnet Synchronous Machines." San José State University, E345, Sep. 21, 2013.

P. Hsu. EE 237. Class Lecture, Topic: "Induction Machines." San José State University, E345, Oct. 5, 2013.

- Kable. "Personal Rapid Transit, South Korea." Internet: <http://www.railway-technology.com/projects/personal-rapid-transit/personal-rapid-transit7.html>, 2014. [Nov. 30, 2014.]
- H.W. Lee, C. Park, et al. "Optimal-Airgap Control of a Linear Induction Motor for Korean Railway Transit." Korea Railroad Research Institute, Dongguk University, Seoul, Korea, 2008.
- Chan-Bae Park; Byung-Song Lee; Hyung-Woo Lee; Kwon, S.-Y.; Hyun-June Park, "Air-gap control system of a linear induction motor for a railway transit," *Electrical Machines, 2008. ICEM 2008. 18th International Conference on*, vol., no., pp.1,4, 6-9 Sept. 2008.
- PRT Consulting. "Gallery: Vectus." Internet: <http://www.prtconsulting.com/gallery7/Photo13.jpg>, 2013, [Nov. 30, 2014].
- P. Sen, *Principles of Electric Machines and Power Electronics, Second Edition*. New York, NY: John Wiley & Sons, Inc., 1996.
- Ultra Global PRT. "Heathrow T5." Internet: [http://www.ultraglobalprt.com/?page\\_id=50](http://www.ultraglobalprt.com/?page_id=50), 2013, [Sep. 6, 2013].
- Ultra Global PRT. "World's first and largest urban PRT system announced." Internet: <http://www.ultraglobalprt.com/worlds-largest-urban-prt-system-announced/>, Dec. 14, 2011, [Sep. 6, 2013].
- United States Department of Energy, Energy Efficiency and Renewable Energy Office. "Energy Conservation Program: Energy Conservation Standards for Commercial and Industrial Electric Motors; Final Rule." Internet: <http://www.regulations.gov/#!documentDetail;D=EERE-2010-BT-STD-0027-0117>, May 29, 2014, [July 17, 2014].
- Vectus. "Suncheon Bay Project, South Korea." Internet: <http://www.vectusprt.com/EN/first-project/>, 2013, [Oct. 13, 2013].
- Vectus. "Vehicle Propulsion." Internet: <http://www.vectusprt.com/EN/propulsion/>, 2012, [Sep. 6, 2013].
- West Virginia University. "Personal Rapid Transit (PRT)." Internet: <http://transportation.wvu.edu/prt>, Nov. 8, 2013, [Nov. 17, 2013].
- T. Wildi. *Electrical Machines, Drives, and Power Systems*. Columbus, OH: Prentice Hall, 2002.
- Wu, Pingbo, et al. "Dynamic Performance of Subway Vehicle with Linear Induction Motor System." *Journal of Mechanical Systems for Transportation and Logistics* 3.1, 2010, pp. 372-379.

## APPENDICES

### Appendix A – Motor configuration calculations

Assumptions were made in the following calculations about motor efficiency and mass added to the vehicle for a given configuration. Adequate data was not yet available regarding rotary motor size and mass, so calculations for a range of increasingly massive units are shown.

	LIM long primary	LIM short primary		Rotary	Rotary	Rotary	Rotary
			<b>Units</b>				
Vehicle mass	1100	1100	kg	1100	1100	1100	1100
Cruise speed	22	22	m/s	22	22	22	22
Aero drag (cruise)	112	112	N	112	112	112	112
Friction drag (cruise)	223	294	N	235	255	274	294
<b>Motor efficiency</b>	<b>0.53</b>	<b>0.80</b>		<b>0.90</b>	<b>0.90</b>	<b>0.90</b>	<b>0.90</b>
Friction coefficient	0.02	0.02		0.02	0.02	0.02	0.02
Regenerative braking recovery	0.60	0.50		0.50	0.50	0.50	0.50
Wheel diameter	0.381	0.381	m	0.381	0.381	0.381	0.381
Cost per kWh	0.231	0.231	\$	0.231	0.231	0.231	0.231
<b>Mass added</b>	<b>0</b>	<b>400</b>	<b>kg</b>	<b>100</b>	<b>200</b>	<b>300</b>	<b>400</b>
Acceleration (normal)	1.125	1.125	m/s <sup>2</sup>	1.125	1.125	1.125	1.125
Deceleration (normal)	1.125	1.125	m/s <sup>2</sup>	1.125	1.125	1.125	1.125
Deceleration (max)	3.000	3.000	m/s <sup>2</sup>	3.000	3.000	3.000	3.000
Time to accelerate:	19.6	19.6	s	19.6	19.6	19.6	19.6
Time to decelerate:	19.6	19.6	s	19.6	19.6	19.6	19.6
Time to emergency stop:	7.3	7.3	s	7.3	7.3	7.3	7.3
Force to cruise:	335	406	N	347.2	366.8	386.4	406
Force to accelerate:	1565	2015	N	1678	1790	1903	2015
Force to decelerate:	1238	1688	N	1350	1463	1575	1688
Force to emergency stop:	3300	4500	N	3600	3900	4200	4500
Torque to accelerate:			Nm	320	341	362	384
Torque to decelerate:			Nm	257	279	300	321
Torque to emergency stop:			Nm	686	743	800	857
distance to accelerate:	215	215	m	215	215	215	215
distance to decelerate:	215	215	m	215	215	215	215
distance to emergency stop:	81	81	m	81	81	81	81
Headway for BWS:	3.7	3.7	s	3.7	3.7	3.7	3.7
Headway for 0.5g stop ahead:	1.4	1.4	s	1.4	1.4	1.4	1.4
Energy to accelerate:	337	434	kJ	361	385	409	434
Energy to brake:	266	363	kJ	290	315	339	363

Energy to emergency stop:	266	363	kJ	290	315	339	363
Power to accelerate:	17.2	22.2	kW	18.5	19.7	20.9	22.2
Power to decelerate:	13.6	18.6	kW	14.9	16.1	17.3	18.6
Power to emergency stop:	36.3	49.5	kW	39.6	42.9	46.2	49.5

**Considering motor efficiency:**

<b>Power required (accelerate):</b>	<b>32.5</b>	<b>27.7</b>	<b>kW</b>	<b>20.5</b>	<b>21.9</b>	<b>23.3</b>	<b>24.6</b>
Power delivered (brake):	4.3	7.4	kW	6.7	7.2	7.8	8.4
Power delivered (emergency):	11.5	19.8	kW	17.8	19.3	20.8	22.3
% of energy recovered:	13%	27%	%	33%	33%	34%	34%
Net energy used:	0.153	0.110	kWh	0.075	0.080	0.084	0.088
<b>Cost per start/stop:</b>	<b>0.035</b>	<b>0.025</b>	<b>\$</b>	<b>0.017</b>	<b>0.018</b>	<b>0.019</b>	<b>0.020</b>

**Cooling required:**

Accelerate:	15.3	5.5	kW	2.1	2.2	2.3	2.5
Decelerate:	9.3	11.1	kW	8.2	8.8	9.5	10.2
Emergency stop:	24.8	29.7	kW	21.8	23.6	25.4	27.2

Single motor cost:	8000	15000	\$	15000	16000	17000	18000
System length:	20	20	km	20	20	20	20
Motor pitch:	1.5		m				
		15	veh/km	15	15	15	15
Motors per vehicle:	0	4		2	2	2	2
Number required:	13333	1200		600	600	600	600
Total motor cost:	106.7	18.0	\$M	9.0	9.6	10.2	10.8

Upfront savings:		88.7	\$M	97.7	97.1	96.5	95.9
------------------	--	------	-----	------	------	------	------

Annualized capital cost:	3.6	1.8	\$M	0.9	1.0	1.0	1.1	at 10% per year
--------------------------	-----	-----	-----	-----	-----	-----	-----	-----------------

## Appendix B – Force Engineering F951 LIM datasheet



### PRODUCT DATA SHEET

Forcepack Type F951

#### General Specification

Description: Three pole linear induction motor  
 Dimensions: 235 x 141 x 44.5 mm overall, 3m leads  
 Nett weight: 6kg approx  
 Insulation, windings: Class H (180C)  
 Insulation, cables, resin: Class H (180C)  
 Protection class: IP60  
 Flammability: UL94-HB  
 Thermal switch type: Single pole, normally closed, automatic reset  
 " " trip temp: 160+/-5C  
 " " contact rating: 1.6A 250v 0.6 p.f. 50/60Hz

Outline Drawing: F951-003

Connection Diagram: F951-003

#### Standard Operating Conditions

Supply frequency: 60 Hz  
 Synchronous speed: 7.2 m/s  
 Reaction plate material: Aluminium extrusion, 6061 grade  
 " " thickness: 3.5 mm  
 " " width: approx. 150 mm  
 " " backiron: 6 x 120 mm mild steel  
 Mechanical clearance: 3 mm maximum

S5 duty in free air at 25C ambient temperature

#### Typical Performance at Ambient

Supply	Speed m/s	Thrust N	Attraction N	Current A	Duty %	Power Factor
208v 3ph	0 – 1	~15	15	~1.0	100+	0.50
208v 3ph	Open motor (No reaction plate)	-	-	0.75	100+	0.15

Insulation tested to 2000 volts AC between all parts.  
 Thermal switch operation checked before despatch.  
 Performance tolerance better than  $\pm 10\%$

Copyright and Confidential

Original Issue 02/04/14

Drawing No. 4f951-001

Gelders Hall Road, Shepshed, Leicestershire, LE12 9NH England  
 Tel: 0 (44) 1509 506 025 Fax: 0 (44) 1509 505 433 Email: enquiries@force.co.uk www.force.co.uk  
 Registered in England, No.1446727

## Appendix C –Emerson Unidrive SP0201 Brochure Excerpt



### The ultimate intelligent AC drive

Performance and flexibility allows you to do something new, creating opportunities to innovate, find better ways to control your application, increase speeds, improve processes and reduce the footprint of your system. Unidrive SP, Control Techniques' high-performance intelligent drive family allows you to achieve this. The ultimate AC drive.

#### One range, any power

Unidrive SP is a complete drive automation range that covers the power spectrum from 0.37kW to 1.9MW. All drives share the same flexible control interface regardless of the power rating. Drives are packaged in three formats: Panel Mount, Free Standing and Modular.

#### Panel Mount – Standard drive modules 0.37kW to 132kW

Unidrive SP panel mount drives are standard AC input, AC output modules for installation within a control panel. The modules are easy to install and commission and can be applied in a wide range of applications.

#### Unidrive SP size 0

is the latest member of the panel mount range. It reduces the drive size by 60% for motors from 0.37kW to 1.5kW. This model has the same parameter set, universal motor control and user interface as the rest of the Unidrive SP range.



#### Free Standing – Ready to run 90kW to 675kW

Unidrive SP Free Standing offers a fully engineered drive that is supplied within a standard sized cabinet. Free Standing can be ordered with input power equipment to facilitate immediate connection to the power supply and motor.

#### Unidrive SP Modular – Power system flexibility 45kW to 1.9MW

Unidrive SP Modular offers maximum power system design flexibility. Drive modules can be connected together in a variety of ways to create common DC bus systems, active input systems for returning excess energy to the power supply and parallel drives for high power motors. All drive modules are compact for easy handling.



[www.controltechniques.com](http://www.controltechniques.com)

## Appendix D – Arduino source code for current data collection

```
/* This sketch implements an inductive current sensors on analog inputs of
an Arduino Pro Mini. Current data is read as an analog voltage and
translated into Amperes, then output via the Serial Monitor. Once current
exceed an established minimum limit, a timer starts. Markers are printed
at the beginning and end of the 2-second window.
written by Erik Aylen
v2.0 13Aug2014
*/

#define PIN_CURRENT_SENSOR_GRID A0
#define PIN_CURRENT_SENSOR_MOTOR A1
#define MOTOR_CURRENT_ZERO_THRESHOLD 0.05
#define RUN_INTERVAL 2000 // run time in milliseconds

float gridCurrentPrevious = 0;
float motorCurrentPrevious = 0;

unsigned long timeStartRun = millis();
boolean running = 0;

void setup ()
{
  Serial.begin (19200);

  pinMode(PIN_CURRENT_SENSOR_GRID, INPUT);
  pinMode(PIN_CURRENT_SENSOR_MOTOR, INPUT);

  Serial.println("Finished setup");
} // end of setup

void loop()
{
  float gridCurrent = analogRead(PIN_CURRENT_SENSOR_GRID)*10.0/1024.0;
  // these sensors measure 0-10A current, hence the 10.0
  float motorCurrent = analogRead(PIN_CURRENT_SENSOR_MOTOR)*10.0/1024.0;
  if ( ( motorCurrentPrevious <= MOTOR_CURRENT_ZERO_THRESHOLD ) && ( motorCurrent >
MOTOR_CURRENT_ZERO_THRESHOLD ) )
  {
    timeStartRun = millis();
    running = 1;
    Serial.println("----- Start Run -----");
  }

  Serial.print(motorCurrent);
  Serial.print(" ");
  Serial.print(gridCurrent);
  Serial.println();

  if ( running && millis() >= timeStartRun + RUN_INTERVAL )
  {
    running = 0;
    Serial.println("----- End Run -----");
  }

  gridCurrentPrevious = gridCurrent;
  motorCurrentPrevious = motorCurrent;
} // end of loop
```

## Appendix E – Arduino source code for motor control

```
// Using code found here:
// http://www.windmeadow.com/node/42#comment-28
// read out a Wii Nunchuck controller
// adapted to work with wireless Nunchuck controllers of third party vendors by Michael Dreher
//

#include <io.h>
#include <interrupt.h>
#include <Wire.h>

#define MIN_SPEED    0
#define MAX_SPEED    255
// these values should be 0 - 255 corresponding to a percentage of the rated speed set in Parameter 0.02

#define DELAY_CBUTTON_HOLD 700

#define DELAY_STOP    50

#define BEGIN_RAMP    1    // most testing run at 190, closed loop at 1
#define DURATION_RAMP 2500 // most testing run at 2500
#define END_RAMP      105  // most testing run at 255, closed loop at 105
                          // the Arduino ramp runs 2.5s but data collection lasts only 2s
                          // the 105 value will give 85/255 (20Hz) at 2s
                          // with synchronous speed set to 60 Hz on the VFD, the 190/255 ramp gives 45 - 60 Hz ramp

#define WIDTH_DEAD_ZONE 6

#define LIMIT_FORWARD_LOWER 128+WIDTH_DEAD_ZONE/2
#define LIMIT_FORWARD_UPPER 255
#define LIMIT_BACKWARD_LOWER 0
#define LIMIT_BACKWARD_UPPER 128-WIDTH_DEAD_ZONE/2

#define PIN_CURRENT_SENSOR_GRID    A0
#define PIN_CURRENT_SENSOR_MOTOR  A1

// pins A4-A5 are used for the wiiChuck connector through the Arduino Wire library

#define PIN_ENABLE    8
#define PIN_ANALOG_SPEED 3
#define PIN_FORWARD  4
#define PIN_BACKWARD 9

#define PRESSED    0
#define NOT_PRESSED 1

#define WII_IDENT_LEN    ((byte)6)
#define WII_TELEGRAM_LEN ((byte)6)
#define WII_NUNCHUCK_TWI_ADR ((byte)0x52)

byte outbuf[WII_TELEGRAM_LEN];    // array to store Arduino output

int joyX    = 0;
int joyY    = 0;
int accelX  = 0;
int accelY  = 0;
int accelZ  = 0;
```

```

int zButton          = 0;
int cButton          = 0;

unsigned long cButtonPressStart = millis();
int    cButtonToggleMarker = 0;
int    cButtonPrevious = 0;

unsigned long runStartTime = 0;

unsigned long startTime = 0;

void setup ()
{
  Serial.begin (19200);

  pinMode(PIN_ENABLE,          OUTPUT);
  pinMode(PIN_ANALOG_SPEED,    OUTPUT);
  pinMode(PIN_FORWARD,        OUTPUT);
  pinMode(PIN_BACKWARD,       OUTPUT);
  digitalWrite(PIN_ENABLE,    LOW);
  digitalWrite(PIN_ANALOG_SPEED, LOW);
  digitalWrite(PIN_FORWARD,   LOW);
  digitalWrite(PIN_BACKWARD,  LOW);

  pinMode(PIN_CURRENT_SENSOR_GRID,  INPUT);
  pinMode(PIN_CURRENT_SENSOR_MOTOR, INPUT);

  delay(100); // wait for things to stabilize

  Wire.begin(); // initialize i2c
  // we need to switch the TWI speed, because the nunchuck uses Fast-TWI
  // normally set in hardware\libraries\Wire\utility\twi.c twi_init()
  // this is the way of doing it without modifying the original files
  #define TWI_FREQ_NUNCHUCK 400000L

  nunchuckInit(0); // send the initialization handshake
  startTime = millis();

  Serial.println("Finished setup");

  } // end of setup

void loop()
{
  displayCurrentSensorData();          //////////////////////////////////////
  getChuckData();
  if( (cButton == PRESSED) && (cButtonPrevious == NOT_PRESSED) )
  {
    cButtonToggleMarker=1;
  }
  if(cButton == NOT_PRESSED)
  {
    cButtonPressStart = millis();
  }

  if (zButton == PRESSED) // zButton is run
  { //run the motor
    setMotorSpeed();
  }

  else if ( millis() >= cButtonPressStart + DELAY_CBUTTON_HOLD )
  { // if cButton has been held long enough
    doFullRun();
  }
}

```



```

Wire.beginTransmission (WII_NUNCHUCK_TWI_ADR);          // transmit to device 0x52
Wire.write (0xF0);          // writes memory address
Wire.write (0x55);          // writes data.
if(Wire.endTransmission() == 0)          // stop transmitting
{
Wire.beginTransmission (WII_NUNCHUCK_TWI_ADR);          // transmit to device 0x52
Wire.write (0xFB);          // writes memory address
Wire.write (0x00);          // writes sent a zero.
if(Wire.endTransmission() == 0)          // stop transmitting
{
rc = 0;
}
}
}
}
while (rc != 0 && (!timeout || ((millis() - time) < timeout)));

return rc;
} // end nunchuckInit

// params:
// ident [out]: pointer to buffer where 6 bytes of identification is stored. Buffer must be at least 6 bytes long.
// A list of possible identifications can be found here: <http://wiibrew.org/wiki/Wiimote#The_New_Way>
// return: 0 == ok, 1 == error
byte readControllerIdent(byte* pIdent)
{
byte rc = 1;

// read identification
Wire.beginTransmission (WII_NUNCHUCK_TWI_ADR); // transmit to device 0x52
Wire.write (0xFA); // writes memory address of ident in controller
if(Wire.endTransmission () == 0) // stop transmitting
{
byte i;
Wire.requestFrom (WII_NUNCHUCK_TWI_ADR, WII_TELEGRAM_LEN); // request data from nunchuck
for (i = 0; (i < WII_TELEGRAM_LEN) && Wire.available (); i++)
{
pIdent[i] = Wire.read(); // read byte as an integer
}
if(i == WII_TELEGRAM_LEN)
{
rc = 0;
}
}
}
return rc;
}

void clearTwilnputBuffer() // clear the read buffer from any partial data
{
while(Wire.available ())
Wire.read();
} // end of clearTwilnputBuffer

void sendZero ()
{
// I don't know why, but it only works correct when doing this exactly 3 times
// otherwise only each 3rd call reads data from the controller (countBytesReceived will be 0 the other times)
for(byte i = 0; i < 3; i++)
{
Wire.beginTransmission (WII_NUNCHUCK_TWI_ADR); // transmit to device 0x52
Wire.write (0x00); // writes one byte
Wire.endTransmission (); // stop transmitting
}
} // end sendZero

```

```

void processChuckData()
{
  // accel data is 10 bits long
  // so we read 8 bits, then we have to add
  // on the last 2 bits. That is why I
  // multiply them by 2 * 2

  joyX = outbuf[0];
  joyY = outbuf[1];
  accelX = outbuf[2] * 2 * 2;
  accelY = outbuf[3] * 2 * 2;
  accelZ = outbuf[4] * 2 * 2;

  zButton = 0;
  cButton = 0;

  // byte outbuf[5] contains bits for z and c buttons
  // it also contains the least significant bits for the accelerometer data
  // so we have to check each bit of byte outbuf[5]
  if ((outbuf[5] >> 0) & 1)
  {
    zButton = 1;
  }

  if ((outbuf[5] >> 1) & 1)
  {
    cButton = 1;
  }

  if ((outbuf[5] >> 2) & 1)
  {
    accelX += 2;
  }
  if ((outbuf[5] >> 3) & 1)
  {
    accelX += 1;
  }

  if ((outbuf[5] >> 4) & 1)
  {
    accelY += 2;
  }
  if ((outbuf[5] >> 5) & 1)
  {
    accelY += 1;
  }

  if ((outbuf[5] >> 6) & 1)
  {
    accelZ += 2;
  }
  if ((outbuf[5] >> 7) & 1)
  {
    accelZ += 1;
  }

} // end of processChuckData

void printChuckData()
{
  // Print the input data we have recieved
  Serial.print (joyX, DEC);
  Serial.print ("\t");

```

```

Serial.print (joyY, DEC);
Serial.print ("\t");

Serial.print (accelX, DEC);
Serial.print ("\t");

Serial.print (accelY, DEC);
Serial.print ("\t");

Serial.print (accelZ, DEC);
Serial.print ("\t");

Serial.print (zButton, DEC);
Serial.print ("\t");

Serial.print (cButton, DEC);
Serial.print ("\t");

//Serial.print ("\r\n");
} // end of printChuckData

void setMotorSpeed()
{
// joyY direction determines direction (set controller pins for direction)
// joyY magnitude determines speed (analogWrite to controller analog input)

digitalWrite(PIN_ENABLE, HIGH);
if (joyY >= LIMIT_FORWARD_LOWER)
{
int forwardSpeed = map(joyY, LIMIT_FORWARD_LOWER, LIMIT_FORWARD_UPPER, MIN_SPEED, MAX_SPEED);
forwardSpeed = constrain(forwardSpeed, 0, 255);
digitalWrite(PIN_BACKWARD, LOW);
digitalWrite(PIN_FORWARD, HIGH);
analogWrite(PIN_ANALOG_SPEED, forwardSpeed);
// Serial.println(forwardSpeed);////////////////////////////////////
}

else if (joyY <= LIMIT_BACKWARD_UPPER)
{
int backwardSpeed = map(joyY, LIMIT_BACKWARD_LOWER, LIMIT_BACKWARD_UPPER, MAX_SPEED, MIN_SPEED);
backwardSpeed = constrain(backwardSpeed, 0, 255);
digitalWrite(PIN_FORWARD, LOW);
digitalWrite(PIN_BACKWARD, HIGH);
analogWrite(PIN_ANALOG_SPEED, backwardSpeed);
// Serial.println(backwardSpeed);////////////////////////////////////
}

else
{
digitalWrite(PIN_ANALOG_SPEED, LOW);
digitalWrite(PIN_FORWARD, LOW);
digitalWrite(PIN_BACKWARD, LOW);
}

} // end setMotorSpeed

void doFullRun()
{
if(cButtonToggleMarker == 1)
{
runStartTime = millis();

if (joyY >= LIMIT_FORWARD_LOWER)

```

```

{
  Serial.println("Start run");
  digitalWrite(PIN_ENABLE, HIGH);
  digitalWrite(PIN_BACKWARD, LOW);
  digitalWrite(PIN_FORWARD, HIGH);

  while( millis() < runStartTime + DURATION_RAMP )
  {
    int motorSpeed = BEGIN_RAMP + ( ( millis() - runStartTime ) / ( DURATION_RAMP * 1.0 ) * ( END_RAMP - BEGIN_RAMP ) );
    motorSpeed = constrain(motorSpeed, 0, 255);
    // Serial.print(motorSpeed);
    // Serial.print("\t");
    analogWrite(PIN_ANALOG_SPEED, motorSpeed);
    displayCurrentSensorData();////////////////////////////////////
  }

  digitalWrite(PIN_FORWARD, LOW);
  digitalWrite(PIN_ANALOG_SPEED, LOW);
  delay(DELAY_STOP);
  digitalWrite(PIN_ENABLE, LOW);
  Serial.println("End run");
}

else if (joyY <= LIMIT_BACKWARD_UPPER)
{
  Serial.println("Start run");
  digitalWrite(PIN_ENABLE, HIGH);
  digitalWrite(PIN_BACKWARD, HIGH);
  digitalWrite(PIN_FORWARD, LOW);

  while( millis() < runStartTime + DURATION_RAMP )
  {
    int motorSpeed = BEGIN_RAMP + ( ( millis() - runStartTime ) / ( DURATION_RAMP * 1.0 ) * ( END_RAMP - BEGIN_RAMP ) );
    motorSpeed = constrain(motorSpeed, 0, 255);
    // Serial.print(motorSpeed);
    // Serial.print("\t");
    analogWrite(PIN_ANALOG_SPEED, motorSpeed);
    displayCurrentSensorData();////////////////////////////////////
  }

  digitalWrite(PIN_BACKWARD, LOW);
  digitalWrite(PIN_ANALOG_SPEED, LOW);
  delay(DELAY_STOP);
  digitalWrite(PIN_ENABLE, LOW);
  Serial.println("End run");
}

else {} // if joystick is in the dead zone, do nothing

cButtonToggleMarker = 0;
}

} // end doFullRun

void setZeroSpeed()
{
  digitalWrite(PIN_ANALOG_SPEED, LOW);
  digitalWrite(PIN_FORWARD, LOW);
  digitalWrite(PIN_BACKWARD, LOW);
  delay(DELAY_STOP);
  digitalWrite(PIN_ENABLE, LOW);
} // end setZeroSpeed

```

## APPENDIX F – MATLAB code for data processing and plotting

```
clc
clear all
tic

numberOfSets      = 8;      % number of datasets to plot together
numberOfFiles     = 18;    % number of data files in a set - 18 gives
                        % mean within 1.0 sigma with 90% confidence
samplingRate      = 75;    % data sample rate in Hz
testInterval      = 2;    % length of collection window in seconds
positiveThreshold = 0.01; % minimum acceleration value considered
                        % positive

% Find beginning and end of forward portion of each run
firstPositiveIndex = zeros(numberOfFiles,1);
%stores index of beginning of each run
runLength          = floor(samplingRate * testInterval);
%calculate number of data points per run
allGapMSS          = zeros(runLength,numberOfFiles,numberOfSets);
%stores all values for all runs
thisRun            = zeros(runLength,1);
%stores all values for current run

for h = 1:numberOfSets
    for i = 1:numberOfFiles
        currentFile = sprintf('%dclg%d.txt',h+1,i); %set filename from 2 to 9
        inputFile   = csvread(currentFile,2,0);    %read data into matrix
        lowPassData = inputFile(:,5);             %extract low-pass column

        for j = 1:size(lowPassData,1) %find index of first positive value
            if (lowPassData(j) >= positiveThreshold)
                firstPositiveIndex(i) = j;
                break
            end
        end

        for k = firstPositiveIndex(i):firstPositiveIndex(i) + runLength - 1 %extract
            positive values
                thisRun(k-firstPositiveIndex(i)+1) = lowPassData(k);
        end

        for n = runLength:-1:1
            if(thisRun(n) < 0)
                thisRun(n) = 0;
            else
                break
            end
        end
    end

    allGapMSS(1:runLength,i,h) = thisRun .* 9.81;
    %store all runs in one matrix
end
end
toc

% allGapMSS = (1:runLength , 1:numberOfFiles , 1:numberOfSets)
% allGapMSS = (1:150 , 1:18 , 1:8 )

%% Efficiency calculations

setAverageAcceleration = zeros(runLength,numberOfSets);
setAverageVelocity     = zeros(runLength,numberOfSets);
setAveragePosition     = zeros(runLength,numberOfSets);
mechanicalPower        = zeros(runLength,numberOfSets);
gapCurrent              = csvread('gapCurrentData.csv');
resistance              = 40; %measured phase resistance of LIM (Ohms)
bogiemass               = 10.17; %measured mass of bogie (kg)
```

```

%computes power from  $P = I^2 * R$ 
iSquared = gapCurrent .* gapCurrent;
powerI2R = iSquared * resistance;

% computes 'typical' runs by averaging all runs for each gap setting
for p = 1:numberOfSets
    for q = 1:runLength
        setAverageAcceleration(q,p) = mean(allGapMSS(q, :, p));
    end
end

sampleTime = testInterval/runLength;

for p = 1:numberOfSets
    previousVelocity = 0;
    previousPosition = 0;
    for q = 1:runLength
        setAverageVelocity(q,p) = previousVelocity + (setAverageAcceleration(q,p) *
sampleTime);
        setAveragePosition(q,p) = previousPosition + (setAverageVelocity(q,p) *
sampleTime);
        previousVelocity = setAverageVelocity(q,p);
        previousPosition = setAveragePosition(q,p);
    end
end

% Power = work / time
% Work = force * distance
% Force = mass * acceleration
% so, for a given point 1:150, power is (M * a * x)/sampleTime
% Electrical efficiency = mechanical power / electrical power
% efficiency = ^^/powerI2R

for p = 1:size(powerI2R,2) %powerI2R missing data for gap=4mm
    for q = 2:size(powerI2R,1)
        %normally would be runLength, but powerI2R was too short
        mechanicalPower(q,p) = (bogieMass * setAverageAcceleration(q,p)...
            *(setAveragePosition(q,p)-setAveragePosition(q-1,p)))/sampleTime;

        efficiency(q,p) = mechanicalPower(q,p) / powerI2R(q,p);
    end
end

timeSeconds = linspace(0,testInterval,size(efficiency,1));

figure
hold on
plot(timeSeconds,efficiency*100)
title('Overall LIM Efficiency','FontSize',14)
xlabel('Time (seconds)','FontSize',12)
ylabel('Efficiency (percent)','FontSize',12)
set(gca,'Color', [.95 .95 .95])
set(gcf,'Color', [1 1 1])

velocityTrimmed = zeros(size(setAverageVelocity,1),size(setAverageVelocity,2)-
1);
velocityTrimmed(:,1:2) = setAverageVelocity(:,1:2);
velocityTrimmed(:,3:end) = setAverageVelocity(:,4:end);

figure
hold on
plot(velocityTrimmed(1:size(efficiency,1),:),efficiency*100)
title('Efficiency vs. Velocity','FontSize',14)
xlabel('Velocity (meters per second)','FontSize',12)
ylabel('Efficiency (percent)','FontSize',12)
set(gca,'Color', [.95 .95 .95])
set(gcf,'Color', [1 1 1])

%% Watts per Newton
%the current data is missing 4mm gap, so powerI2R is as well

```

```

%the force data needs a column removed to match power

setAverageForce = bogieMass * setAverageAcceleration;
forceTrimmed(:,1:2)=setAverageForce(:,1:2);
forceTrimmed(:,3:end)=setAverageForce(:,4:end);

wattsPerNewton = powerI2R ./ forceTrimmed(1:146,:);

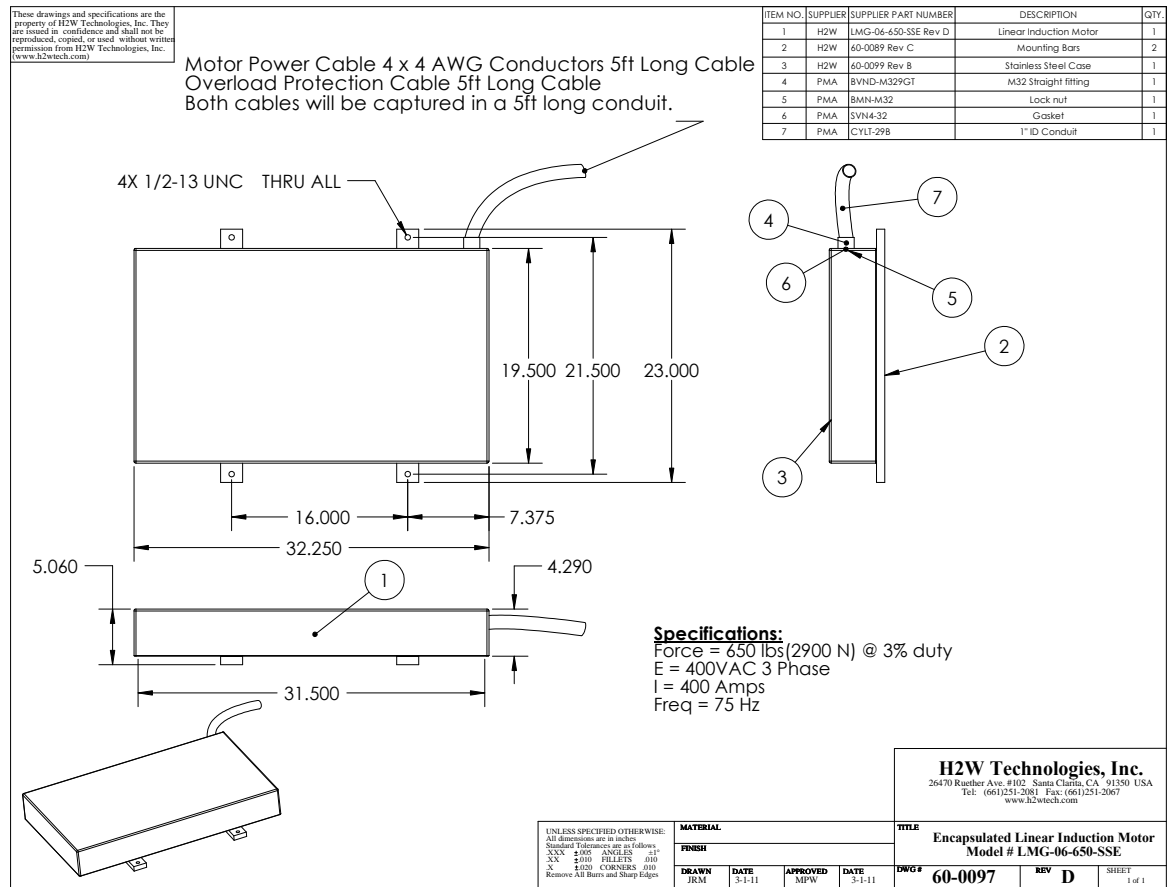
figure
hold on
plot(timeSeconds,wattsPerNewton)
title('Watts per Newton','FontSize',14)
xlabel('Time (seconds)','FontSize',12)
ylabel('Watts per Newton','FontSize',12)
set(gca,'Color',([.95 .95 .95]))
set(gcf,'Color',[1 1 1])

```

## APPENDIX G – Sample regression model coefficients

Time (s)	$x^3$	$x^2$	$x$	$c$
0.013	0.000136379	-0.001543842	-0.00273856	0.157890717
0.027	-0.000508947	0.010888198	-0.075128313	0.289818763
0.040	9.90E-05	0.001437762	-0.035350951	0.273302019
0.053	-0.000146631	0.006414475	-0.067775155	0.353168383
0.067	-0.000274285	0.010248816	-0.102391128	0.465893691
0.080	-0.000891799	0.021248817	-0.162272397	0.578880418
0.093	-0.001196516	0.027893132	-0.207844975	0.693161338
0.107	-0.001625348	0.035609398	-0.25156161	0.786304602
0.120	-0.002393862	0.049979562	-0.337522716	0.968301669
0.133	-0.002870949	0.058429943	-0.383560263	1.063782723

## APPENDIX H – H2W LMG-06-650-SSE LIM datasheet



Specifications:

Description: 6 pole AC linear induction motor encapsulated in a stainless steel enclosure  
Air gap between top of motor and bottom of aluminium plate = 0.625"  
Force: 650lbs (2900 N) @ 3% duty  
Requires: 3 phase 400V AC 475A@45-75Hz  
Dimensions: 5.063" H x 23" W x 32.25"  
Net Weight: approximately 480 lbs (220 kg)  
Insulation, windings: Class H (180 °C) insulation, cables, resin: Class F (155 °C)  
Proection Class: Encapsulated in 5 sided 300 series stainless steel box

Thermal switch trip temp.: 140 °C  
Thermal switch contact rating: 1.6A 250v 0.6p.f. 50/60Hz

Cables" Power leads are four 5 ft long 4 AWG Motor power leads, two thermal switches, 5 feet long with shield and contained in a 1" OD splash resistant conduit

TITLE: <b>Encapsulated Linear Induction Motor Model # LMG-06-650-SSE</b>		
DWG #	REV	SHEET
<b>60-0097</b>	<b>D</b>	2 of 2